8-25-2022

# Multi-OMICs analysis reveals metabolic and epigenetic changes associated with macrophage polarization

Mark L. Sowers

Hui Tang

Vipul K. Singh

Arshad Khan

Abhishek Mishra

*See next page for additional authors*

## Authors

Mark L. Sowers, Hui Tang, Vipul K. Singh, Arshad Khan, Abhishek Mishra, Blanca I. Restrepo, Chinnaswamy Jagannath, and Kangling Zhang

Journal Pre-proof

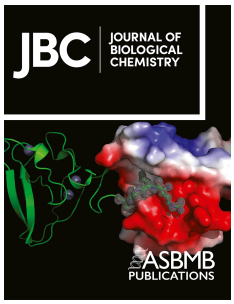


# Multi-OMICs analysis reveals metabolic and epigenetic changes associated with macrophage polarization

Mark L. Sowers, Hui Tang, Vipul K. Singh, Arshad Khan, Abhishek Mishra, Blanca I. Restrepo, Chinnaswamy Jagannath, Kangling Zhang

PII: S0021-9258(22)00861-4

DOI: https://doi.org/10.1016/j.jbc.2022.102418

Reference: JBC 102418

To appear in: *Journal of Biological Chemistry*

Received Date: 25 February 2022

Revised Date: 20 August 2022

Accepted Date: 22 August 2022

Please cite this article as: Sowers ML, Tang H, Singh VK, Khan A, Mishra A, Restrepo BI, Jagannath C, Zhang K, Multi-OMICs analysis reveals metabolic and epigenetic changes associated with macrophage polarization, *Journal of Biological Chemistry* (2022), doi: https://doi.org/10.1016/j.jbc.2022.102418.

# CRediT author statement

MLS, HT, VKS, AK and AM conducted experiments and acquiring data; BIR provided reagents and advice. KZ designed and analyzed data, CJ designed experiments and edited the manuscript.

# Multi-OMICs analysis reveals metabolic and epigenetic changes associated with macrophage polarization

Subtitle: *Metabolism and histone modification crosstalk during MΦ polarization*

Mark L. Sowers[1], Hui Tang[1], Vipul K. Singh[2], Arshad Khan[2], Abhishek Mishra, Blanca I Restrepo[3], Chinnaswamy Jagannath[2,*], and Kangling Zhang[1,*]

[1]*Dept. of Pharmacology and Toxicology, University of Texas Medical Branch, Galveston, TX*
[2]*Dept. of Pathology and Genomic Medicine, Center for Molecular and Translational Human Infectious Diseases Research Houston Methodist Research Institute, Weill-Cornell Medicine, Houston, TX.*
[3]*UT School of Public Health, Brownsville, TX*

**Correspondence to*:

**Kangling Zhang, Ph.D**., Associate Professor, Dept. of Pharmacology and Toxicology, University of Texas Medical Branch, Galveston, TX 77555.
Email: kazhang@utmb.edu

*Co-corresponding author:*

Chinnaswamy Jagannath. Ph.D., Professor, Dept. of Pathology and Genomic Medicine, Houston Methodist Research Institute, Weill Cornell Medicine, Houston, TX 77030. Email: cjagannath@houstonmethodist.org

**ABSTRACT**

Macrophages (MΦ) are an essential immune cell for defense and repair that travel to different tissues and adapt based on local stimuli. A critical factor that may govern their polarization is the cross-talk between metabolism and epigenetics. However, simultaneous measurements of metabolites, epigenetics, and proteins (phenotype) has been a major technical challenge. To address this, we have developed a novel triomics approach using mass spectrometry to comprehensively analyze metabolites, proteins, and histone modifications, in a single sample. To demonstrate this technique, we investigated the metabolic-epigenetic-phenotype axis following polarization of human blood-derived monocytes into either 'pro-inflammatory M1'- or 'anti-inflammatory M2-' MΦs. We report here a complex relationship between arginine, tryptophan, glucose, and the citric acid cycle (TCA) metabolism, protein and histone post-translational modifications, and human macrophage polarization that was previously not described. Surprisingly, M1-MΦs had globally reduced histone acetylation levels but high levels of acetylated amino acids. This suggests acetyl-CoA was diverted, in part, towards acetylated amino acids. Consistent with this, stable isotope tracing of glucose revealed reduced usage of acetyl-CoA for histone acetylation in M1-MΦs. Furthermore, isotope tracing also revealed MΦs uncoupled glycolysis from the TCA cycle, as evidenced by poor isotope enrichment of succinate. M2-MΦs had high levels of kynurenine and serotonin which are reported to have immune-suppressive effects. Kynurenine is upstream of *de novo* $NAD^+$ metabolism which is a necessary cofactor for Sirtuin-type histone deacetylases. Taken together, we demonstrate a complex interplay between metabolism and epigenetics that may ultimately influence cell phenotype.

**INTRODUCTION**

Macrophages (MΦs) are essential phagocytes that mediate antimicrobial immunity. Mϕ precursors, monocytes, enter circulation and home to tissues where they differentiate into tissue-specific MΦs that express distinct markers. Multiple phenotypes have been described that perform site-specific functions depending on the tissue environment (1-3). MΦ differentiation and activation is a complex process involving orchestrated signaling induced by cytokines, chemokines, and interactions with pathogen-associated molecular patterns (PAMPs) and damage-associated molecular patterns (DAMPS) (4). Classically, activated MΦs are 'pro-inflammatory' and referred to as M1-MΦs, whereas alternatively activated MΦs are 'anti-inflammatory' and referred to as M2-MΦs (5). M1-MΦs can be induced by IFN-γ from monocytes or resting MΦs (M0-MΦ), and M2-MΦs are induced by IL-4, IL-10, and IL-13 (6). In addition, multiple subsets of M2-MΦs (M2a, M2b, and M2c) have also been described (7).

MΦ polarization helps the immune system balance between the need to kill pathogens (M1-MΦs) and to perform repair following infection- and cytokine-related damage (M2-MΦs) (8). Improper MΦ polarization can contribute to the pathophysiology of metabolic syndrome (9-11), infectious and autoimmune diseases (12), asthma (13), and cancer (10,14). A better understanding of MΦ polarization may allow us to develop therapeutic strategies for tuning polarization.

Recent studies have shed some light on the interplay that exists between epigenetics and metabolism that may be involved or even govern macrophage polarization (15,16). Previous studies, primarily using mouse MΦs, show a striking contrast between transcriptional and metabolic profiles between M1- and M2-MΦs (10,17-20). Typically iNOS is reported to be upregulated in M1-MΦs resulting in arginine catabolism to citrulline and nitric oxide, as well as produce reactive oxygen and nitrogen species (21). In contrast M2-MΦs, instead convert arginine into ornithine and urea using ARG1. Furthermore, M1-MΦs are characterized by enhanced glycolysis, an upregulated pentose phosphate pathway (PPP), and

decreased oxidative phosphorylation (OxPhos) while M2-MΦs are characterized by largely the opposite (11,19,22). Furthermore, metabolites and nutrients in the microenvironment, including amino acids, glucose, fatty acids, hormones, vitamins, and even oxygen, can further influence polarization (23-29).

Histone epigenetic regulation can directly influence gene expression. Enzymes that add or remove these modifiers to chromatin alter the physical accessibility of a set of genes and their promoters which can directly influence gene expression (30,31). Both mathematical models and experimental observations confirm acetylation changes occur depending upon the metabolic state. For example, a shift from low to high glucose significantly affects histone acetylation levels, as do changes in acetate, hypoxia, or starvation of certain amino acids (32-37). Histone acetylation and methylation are dependent upon their required acetyltransferase and methyltransferase cofactors, acetyl-CoA and S-adenosylmethionine (SAM), respectively. Acetyl-CoA is derived from pyruvate, the final product of glycolysis, as well as β-oxidation of fatty acids. SAM is formed from methionine which can be imported or synthesized from homocysteine and 5-methyltetrahydrofolate (5-methylTHF), which requires $B_{12}$ and folate. Serine, or glucose derived serine, is the source of carbon for 5-methylTHF. Consequently, epigenetic markers are a direct consequence of multiple overlapping metabolic pathways that are differentially activated in polarized macrophages.

While epigenetic regulation is closely tied to the synthesis and availability of the necessary cofactors, other factors produced by macrophages or in the microenvironment can further influence epigenetics. As an example, vitamin $B_{12}$ can be irreversibly bound to NO, which is upregulated in M1-MΦs and inhibits *de novo* methionine synthesis (38-41). In addition, others have demonstrated that itaconic acid (19,42,43) can inhibit $B_{12}$-dependent enzymes, and hypoxia can block intracellular uptake of $B_{12}$ (44). In addition, others have demonstrated an accumulation of 5-methylTHF in M2-MΦs relative to M1-MΦs (45).

Previous approaches to measure metabolites, epigenetics, and protein expression (phenotype) have required multiple techniques and a variety of instruments including one or more kinds of mass spectrometers, western blot, qPCR, and other techniques. Each of these approaches are specialized and thus can limit the study of the metabolic-epigenetic-phenotype axis. Herein, we describe a novel triomics method to simultaneously analyze metabolites, histone modifications (epigenetics), and protein expression (phenotype) using MΦs polarized *in vitro*. Secondly, we describe a mass spectrometric method to trace glucose incorporation into histone modifications (acetylation) that is based on our previous report of tracing histone methylation derived from serine (46). Our work described herein provides an analytical platform to study the complex crosstalk between metabolism, epigenetics, and cell plasticity. We demonstrate this by applying our approach to study MΦ polarization

## RESULTS

### *Triomics-analysis of metabolites, proteins, and histone modifications*

**Figure 1** outlines our Triomics workflow where we extract proteins, metabolites, and histones from single samples. After isolating each material, we can visualize differential expression with a volcano plot comparing M1- and M2-MΦs (**Figure 2A)**. A total of 112 metabolites were identified and quantified. The authenticity of metabolites was determined based on the accuracy of the precursor ions, which was set at a threshold of 5.0 ppm. The majority were further validated by MS2 fragment ions that corresponded to their chemical structures.

A total of 15 modified histone peptides were quantified (**Figure S1**). **Figure 2B** shows a volcano plot displaying the fold changes of modifications in M2-MΦs versus M1-MΦs with significance (p-value) of change calculated from up to 8 measurements of a pooled sample containing 3 biological samples. The data demonstrate that acetylation of histone H3 and H4 at all sites was consistently higher in M2-MΦs than in M1-MΦs. Additionally, dipeptide acetylation of KS and KG, detected in our metabolomics assay, was higher in M2-MΦs than in M1-MΦs. This suggests that these acetylated dipeptides could be degradation products of acetylated proteins (**Figure 2A**).

As for methylated histone modifications, H3K4me3 was significantly higher in M1-MΦs than M2-MΦs. Methylation at other sites including H3K9 (mono-, di-, and trimethylation), H3K27 trimethylation, H3K36 mono-methylation, K79 mono-methylation, H4K20 mono-, di, and trimethylation was either lower in M1-MΦs compared to M2-MΦs or unchanged between them (**Figure 2B & S1**). This suggests that there are significant alterations to the histone epigenetic code between M1- and M2-MΦs, with histone acetylation broadly being elevated in M2-MΦs and methylation being downregulated or unchanged.

A total of 2937 proteins were quantified with statistical significance (q-value ≤ 0.05). **Figure 2C** is a volcano plot showing the relationship of $\log_2$ fold change of proteins differentially expressed in M2-MΦs versus M1-MΦs and their statistical significance. 866 proteins were downregulated (blue) and 710 proteins were upregulated (red) in M2-MΦs versus M1-Mφs by >1.25 fold. **Figure 2D** illustrates a heatmap of protein expression in M1- and M2-MΦs compared to M0-MΦs and between M1- and M2-MΦs. Among the 10 most upregulated proteins, LGALS3/Galectin 3 was elevated in M1-MΦs, consistent with our previous RNA-seq analysis (47). LGALS3 is associated with autophagy-dependent antibacterial activity (48). Also, consistent with our transcriptome analysis, RelA was significantly upregulated in M1-MΦs whereas SIRT2 was upregulated in M2-MΦs. SIRT2 is known to regulate the expression of RelA deacetylation, thereby modulating its function (49).

We then took the differentially expressed proteins for pathway enrichment analysis, using g:Profiler and Cytoscape with EnrichmentMap for visualization (50). IFN-γ signaling, response to type I interferon, NADH-respiratory chain complex 1, MHC-I dependent antigen processing, glycolysis, and ROS/NOS in phagocytes were among the enriched pathways in M1-MΦs (**Figure 3A**). In comparison, antigen presentation MHC class II, tricarboxylic acid (TCA) cycle, and oxidative phosphorylation (oxPhos) were enriched in M2-MΦs (**Figure 3B**).

***Arginine metabolism and arginine methylation***

iNOS is a hallmark in activated M1-MΦ's. iNOS consumes arginine and metabolizes it to citrulline, producing nitric oxide (NO). On the other hand, M2-MΦs are frequently defined by the high expression of ARG1, which instead metabolizes arginine into ornithine and urea. While ornithine was elevated in M2-MΦs, we did not see higher citrulline in M1-MΦs as expected. Instead, both citrulline and ornithine were significantly higher in M2-MΦs (**Figure 4A-B**). Despite this, we found evidence of NO oxidation in M1-MΦs. We detected the Nitric oxide synthase intermediate, $N^G$-hydroxy-arginine (NOHA), although it was not significantly different between different MΦs. However, NO can also react with tyrosine to form nitrotyrosine which was also found significantly higher in M1- compared to M2-MΦs (**Figure 4A**). The high levels of citrulline in M2-MΦs, rather than in the M1-MΦs, are best explained by ornithine conversion into citrulline by ornithine transcarbamylase (OTC). Ornithine can then be metabolized to pyrroline 5-carboxylate (P5C), which can be further metabolized into proline or glutamate (**Figure 4A-B**). Overall, we find that M2-MΦs elevate ornithine and citrulline levels likely due to conversion of arginine to ornithine and ornithine to citrulline, by ARG1 and OTC, respectively.

Alternatively, arginine can instead be metabolized to creatine or agmatine. Agmatine was higher in M2-MΦs. Agmatine is a precursor of polyamines which can suppress iNOS expression after inflammation, potentially playing an anti-inflammatory role (51,52). Alternatively, arginine can be combined with glycine to produce ornithine and guanidinoacetate. Guanidinoacetate can then be converted to creatine following methylation using SAM. However, we found creatine levels in M2-MΦs were not statistically different while absolute levels of agmatine were 10-20x higher than creatine. This suggests arginine is preferentially converted to agmatine.

Additionally, arginine residues in proteins can be methylated by arginine methyltransferases (PRMTs). These proteins can be catabolized to produce mono- and dimethylated arginine (Rme1 & Rme2) as well as dipeptides, GRme2 and Rme2G. These were all higher in M1- compared to M2-MΦs (**Figure 4C**). Based on mass spectrometry, arginine dimethylation was predominately asymmetric because the $MH^+$-45 ion (loss of dimethylamine) was detected, but the symmetric demethylation signature $MH^+$-31 ion (loss of methylamine) was not (53). Interestingly mono-methylated arginine, also known as N-mono-methyl-L-arginine (L-NMMA), and asymmetric dimethylated arginine (ADMA) are known to modulate NO production by competing with arginine for NOS binding (54).

In contrast, monomethylated arginine dipeptides, Rme1G and GRme1, were significantly lower in M1-MΦs. We were unable to detect PRMT1, which is the major asymmetric arginine dimethyltransferase (55,56). Protein Arginine Methyltransferase 5 (PRMT5) was the only arginine methyltransferase among PRMT1-8 detected by proteomics and was upregulated in M2-MΦs. PRMT5 can methylate histone H4R3 in the mono- and symmetric dimethylation form to repress gene expression. In addition, previous studies show that PRMT5 can methylate RelA-R30 to regulate the transcription of a subset of TNF-α-induced pro-inflammatory genes, including CXCL10 (57,58). These intriguing data from our metabolic analysis warrant additional studies on the role of arginine metabolism and methylation, especially in the context of histone arginine methylation during MΦ polarization and activation.

***Tryptophan metabolism***

Tryptophan can be metabolized by tryptophan hydroxylase to form 5-hydroxyl-tryptophan (5-HO-Trp) and later form serotonin. Alternatively, indolamine-2,3-dioxygenase 1 (IDO1) can metabolize tryptophan to form N-formyl-Kynurenine and ultimately, Kynurenine. IDO1 has antibacterial and immunosuppressive functions (59). Notably, its product, kynurenine, can mediate antimicrobial functions (60). We found that serotonin concentration was several-fold lower in M0- and M1-MΦs than in M2-MΦ (**Figure 5A**). This could be due to the inhibition of tryptophan hydroxylase (TPH) by NO (**Figure 5B**) (61). A higher level of serotonin in M2-MΦ is consistent with earlier reports that serotonin has anti-inflammatory effects and suppresses the release of TNF-α and IL-1β in immune cells and IFN-γ-induced phagocytosis at high concentrations (62-64).

Kynurenine was dramatically increased in M2-MΦs compared to M0- and M1-MΦs (**Figure 5A**). Kynurenine is known to act on the aryl hydrocarbon receptor, which can dampen the immune system response (65). Kynurenine can be further metabolized into downstream products, including $NAD^+$, a critical energy metabolite for redox reactions, and it serves as the substrate for Sirtuin histone-modifying enzymes. We also detected other products of tryptophan metabolism, including picolinic acid, which was only moderately increased in M1-MΦs (**Figure 5A-B**). We quantified three proteins in the tryptophan metabolic pathway, including kynurenine 3-monooxygenase (KMO), kynureninase (KYNU), and quinolinate phosphoribosyltransferase (QPRT) (**Figure 5C**). KMO expression was decreased by 25% in M1-MΦs compared to M2-MΦs; KYNU expression was comparable, but QPRT expression increased fourfold in M1-MΦs compared to M2-MΦs (**Figure 5C**).

*De novo* $NAD^+$ biosynthesis requires QPRT which was decreased in M2-MΦs. However, M2-MΦs have higher levels of kynurenine and serotonin but lower levels of QPRT protein. This indicates the complex regulation of tryptophan metabolism at the proteomic and metabolomic level. High levels of kynurenine in M2-MΦs might suggest increased NAD+ production as there may be increased utilization of the *de novo* synthesis pathway. However, M1-MΦs may simply have a higher flux through the *de novo* NAD+ pathway and more readily produce $NAD^+$ as an end product. M2-MΦs, on the other hand, may accumulate these precursors which are believed to dampen immune responses (65), at the cost of producing $NAD^+$. Our initial study here cannot determine which possibility is correct although the latter explanation would be consistent with the elevated histone acetylation in M2-MΦs as a lack of NAD+ would provent Sirtuins from deacetylating histones. Further studies directly measuring NAD+ as well as using isotope tracing studies with tryptophan would be required to fully understand the utilization of this pathway.

***Central carbon metabolism and histone acetylation***

Central carbon metabolism refers to the metabolic pathways, including glycolysis, the TCA cycle, and the electron respiratory chain. We successfully quantified nearly all catalytic enzymes in glycolysis using proteomics (**Figure 6A**). The following glycolytic enzymes were elevated in M1-MΦs: phosphoglucomutase 1 (PGM1), triosephosphate isomerase 1 (TPI1), fructose-bisphosphatase 1/2 (FBP1 and FBP2), fructose-bisphosphate aldolase A (ALDOA), and enolase 2 (ENO2). Alternatively, the following glycolytic enzymes were elevated in M2-MΦs: Hexokinase 1/2/3 (HK1, HK2, and HK3), liver type-phosphofructokinase (PFKL), glucose-6-phosphate isomerase (GPI), pyruvate kinase 2 (PKM2), glyceraldehyde-3-phosphate dehydrogenase, and spermatogenic (GAPDHS). Levels of phosphoglucomutase 2 (PGM2), enolase 1 (ENO1), and glyceraldehyde-3-phosphate dehydrogenase (GAPDH) were comparable between the two states. **Figure 6B** displays altered expression profiles of proteins in the TCA cycle and its coupled pyruvate and aspartate/glutamate pathways.

Except for citrate synthase (CS) and malate dehydrogenase 2 (MDH2), which were not differentially expressed, all TCA cycle enzymes detected were upregulated in M2-MΦs. The major enzymes involved in pyruvate metabolism, pyruvate kinase M2 (PKM2), and lactate dehydrogenase A/B (LDHA and LDHB) were upregulated in M2-MΦs, except lactate dehydrogenase D (LDHD) which was upregulated in M1-MΦs. These results are consistent with prior reports of elevated TCA pathway in M2-MΦs.

While glucose is the typical source of carbons for the TCA pathways glutamate can also be used to fuel the TCA cycle. In M1-MΦs we found increased levels of glutamic-oxaloacetic transaminase 1 (GOT1), glutamate dehydrogenase 1(GLUD1), glutamate-ammonia ligase (GLUL), glutaminase (GLS), and solute carrier family 1 member 3 (SLC1A3). These results suggest that M1-MΦs may upregulate glutamine/glutamate incorporation into the TCA cycle rather than glucose.

Consistent with the elevated TCA enzymes in M2-MΦs, we generally observed a corresponding increase in the enzymes involved in oxidative phosphorylation. **Figure 6C** displays altered expression of mitochondrial respiration chain proteins. Mitochondrial electron transport chain complex I (ETC) proteins were unchanged, except for NADH:Ubiquinone Oxidoreductase Complex Assembly Factor 4 (NDUFAF4) which was upregulated in M2-MΦs. Complex II enzymes, Succinate dehydrogenase A and B were comparable between M1- and M2-MΦs. Five members of complex III were upregulated in M2-MΦs, including cytochrome B (CYB)-A, 5A, 5B, 5R1, and 5R3. In contrast, CYBB was solely upregulated in M1-MΦs. Elevated CYBB, also called NOX2, is consistent with reports that it is a primary component of the microbicidal phagocyte oxidase system and generates reactive oxygen species in M1-MΦs (66). The following Cytochrome C oxidases (COX) of complex IV were upregulated in M2-MΦs: COX2 (MT-CO2) fragment, COX5B, COX15, COA3 (COX assembly factor 3), OXA1L (COX assembly 1-like), and TACO1

(translational activator of COX1). On the other hand, COX5A, COX6C, COX7C, and COA5 (COX assembly factor 5) were upregulated in M1-MΦs. ATP synthases are also differentially expressed: ATP5A/B/C/D/L were upregulated in M2-MΦs, whereas ATP5E/G3/I/J were upregulated in M1-MΦs.

All metabolites related to the TCA cycle and its coupled pyruvate and aspartate/glutamate pathways were measured using the O-Benzhylhydroxylamine (O-BHA) derivatization-LC-MS/MS method. Pyruvate (Pyr) and lactate (Lac) concentrations were significantly higher in M1-MΦs. We also found decreased citrate and α-ketoglutarate (α-KG) in M1-MΦs. However, citrate/isocitrate isoforms were not fully resolved by our LC/MS method. These findings are consistent with previous reports that the TCA cycle is blocked before α-KG formation, by inhibition of either IDH or aconitase 2 (ACO2) via NO inhibition (19,67). No differences in succinate or malate concentrations were found in M1- and M2-MΦs (**Figure S2**). However, Oxaloacetate (OAA) was elevated in M1-MΦs (**Figure 2A**), but OAA can be derived from aspartate or glutamate (68). Both Aspartate and Glutamate were significantly higher in M2-MΦs compared to M1-MΦs (**Figure 6D-E**). This may indicate that they accumulate in M2-MΦs but are used in M1-MΦs to form OAA for entry into the TCA cycle.

**Accumulation of acetylated amino acids in M1-MΦs**

Acetylated aspartic acid (NAA) and acetylated glutamate (NAG) were elevated in M1- relative to M2-MΦs (**Figure 2A and 6D-E**). The concentration of NAA was ten times that of NAG, suggesting that NAA is the major pool of acetyl groups. The measured NAA concentration (~0.4 nmol/mg protein in M1-MΦs and ~0.2 nmol/mg protein in M0- and M2-MΦs) was comparable to the concentrations measured in immortalized brown adipocytes (0.1 nmol/mg protein) (69-72). Surprisingly, N-acetyl-ornithine (NAO) was also abundant (**Figure S3**), and its concentration in M1-MΦs was about four times that of M2-MΦs and two times that of M0-MΦs (**Figure 6D-E**). NAO is the metabolic product of NAG (73). We propose that higher levels of NAA, NAG, and NAO in M1-MΦs may function as acetyl-CoA trap that could result in the observed decreases in histone acetylation (**Figure 2A-B**).

**Tracking acetyl groups into histone acetylation**

To better understand how glucose metabolism affects histone acetylation, we performed isotope tracing using uniformly labeled $^{13}C_6$-glucose. Isotope enrichment of pyruvate and lactate was higher in M1-MΦs than M0-MΦs, confirming the upregulation of glycolysis by IFN-γ (**Figure 7A**). However, levels of pyruvate and lactate were higher in M2-MΦ. Unexpectedly the total isotope enrichment of pyruvate was only 1-2% while lactate was 10-15%. This would appear to indicate that pyruvate is being diverted to either lactate or acetyl-CoA. However, we see a similar 1-2% enrichment of succinate suggesting acetyl-CoA is largely not being incorporated into the TCA cycle. Consistent with this, isotope labeled glucose incorporation into H3K18/23 acetylation is enriched by 20-25% which indicated that production of acetyl-CoA is not blocked but rather is diverted to histone acetylation rather than into the TCA cycle (**Figure 7B**).

Decreased enrichment of succinate $M^{+2}$ isotopologue ($^{13}C_2$) (**Figure 7A**) confirms TCA cycle impairment at the formation of α-KG, which is also indicated by proteomics (**Figures 6B**). $^{13}C_2$-acetyl incorporation from glucose to histones was measured as illustrated by **Figure S4**. Enrichment is higher in M1- and further increased in M2-MΦs, compared to M0-MΦs, although the differences are relatively modest (**Figure 7B**). These results are consistent with reduced global histone acetylation in M1-MΦs compared to M2-MΦs in non-isotope tracing experiments (**Figure 2B**).

To examine the effects of hypoxia on histone modifications and isotope incorporation, MΦs were cultured otherwise identically but under hypoxic conditions (2% $O_2$). Levels of H3K18/23Ac isotope enrichment were decreased in M0 and M2- MΦs relative to normoxia. Consequently, the relative enrichment of this

modification is higher in M1-MΦs than either M0 or M2 MΦs under hypoxia. This observation is consistent with a previous report indicating that hypoxia suppresses metabolism through the TCA cycle by trans-activating the gene encoding pyruvate dehydrogenase kinase 1 (*PDK1*). PDK1 then inactivates the Pyruvate Dehydrogenase Complex (PDH) which results in decreased acetyl-CoA formation from glucose metabolism (74). Furthermore, one-carbon metabolism appeared to be inhibited in M1-MΦs as there was reduced methyl transfer from serine to histones. Hypoxia further enhanced this effect (**Figure S5**).

**DISCUSSION**

We have developed an innovative triomics method to understand the crosstalk between metabolism and histone modifications during IFN-γ and IL-4-mediated polarization of human MΦs. From acetone extracts of cell lysate, we were able to quantify hundreds of metabolites containing primary amines or carboxylic acids using dansylation and O-benzylhydroxylamine (O-BHA) derivatization, respectively. The concentrations of the 20 amino acids, modified amino acids/dipeptides, such as methylated lysine and arginine, acetylated lysine and ornithine, arginine and glutamate metabolism, and tryptophan metabolism, were successfully quantified by dansylation derivatization followed by LC-MS/MS analysis. Concentrations of TCA cycle intermediates were measured by O-BHA derivatization followed by LC-MS/MS analysis. We compared their relative concentration levels in M0-, M1-, and M2-MΦs.

In M1-MΦs we saw increased levels of nitrotyrosine supporting their role in producing reactive nitrogen species to combat pathogens. Consistent with the 'anti-inflammatory' role of M2-MΦs, tryptophan and arginine pathways revealed elevated levels of agmatine, serotonin, and kynurenine which are all believed to play some anti-inflammatory role. Additionally, glutathione detoxification was significantly upregulated, and ROS formation is downregulated in M2-MΦs (**Figure S6A**). A corresponding decrease of 4-HNE (**Figure 2A**), a marker as lipid peroxidation, as well as oxidized threonine (AAAS), and lysine (AKBA) was observed (**Figure S6B-C**). However, based on our results at the protein and metabolite level, previous reports that suggest a 'glycolytic' M1 subtype and an 'Oxphos' M2-subtype generalization may be just that, a generalization, and the dynamics of those pathways, and their intersection with MΦ polarization, may be more complex than previously appreciated.

Interestingly, in all MΦ subtypes studied herein, stable-isotope tracing with glucose suggested that very little glucose made its way into the TCA cycle (**Figure 7A**). While the proteomic data suggested that M2-MΦs may upregulate Oxphos, it appears that MΦs overall do not utilize glucose molecules in the TCA cycle. It is possible that the enrichment of succinate is poor, not because the TCA cycle is dysfunctional, but rather that other sources of carbons, such as glutamate, are being preferentially used.

LC-MS/MS analysis demonstrated that histone acetylation was significantly lower in M1-MΦs than M2-MΦs (**Figure 2B**). Our metabolomics data identified an accumulation of N-acetyl-aspartic acid (NAA), N-acetyl-glutamate (NAG), and the NAG metabolic product N-acetylornithine (NAO) in M1-MΦs which may explain the decreased levels of histone acetylation relative to M2-MΦs. Although differential expression of histone acetyltransferases and deacetylases cannot be ruled out, lower acetyl-CoA production from glycolysis and blocked acetyl release from NAA, NAG, and NAO could also explain the epigenetic differences in polarized MΦs.

Importantly, *de novo* synthesis of $NAD^+$ through tryptophan metabolism was significantly upregulated in M1-MΦs, as evidenced by elevated levels of nicotinic acid and significant overexpression of QPRT (**Figure**

**5**). We predict that the production of $NAD^+$ by oxidation of NADH via mitochondrial respiratory complex I is enhanced in M1-MΦs, because most complex I proteins were upregulated (**Figure 6C**). Elevated $NAD^+$ from tryptophan metabolism as well as NADH oxidation may, in turn, enhance the activity of sirtuin-type histone deacetylases, thereby reducing histone acetylation. Our metabolomic approach did not measure $NAD^+$ levels and only provides a snapshot of tryptophan metabolism. Future studies should be done to investigate the mechanism by which we identified higher levels of kynurenine in M2-MΦs, but higher levels of downstream metabolites, closer towards $NAD^+$ synthesis, in M1-MΦs. Tryptophan metabolism may be a major contributor to the respective roles of M1 and M2-MΦs in immune activation.

Because acetyl-CoA can also be produced from fatty acid β-oxidation, we sought to determine whether fatty acid β-oxidation occurs differentially in M0-, M1-, and M2-MΦs (**Figure S6**). Our data suggest that there are no significant differences in fatty acid β-oxidation among the three types of MΦs. Concentrations of middle to long-chain fatty acids, including hexanoic acid, palmitic acid, and palmitoleic acid, were significantly lower in M1-MΦs. If these were degraded by β-oxidation to short-chain fatty acids, we should have detected considerably higher concentrations of acetic and butyric acids. However, this was not found (**Figure S6B-C**). Middle to long-chain fatty acids are likely consumed to synthesize very long chain fatty acids due to upregulation of ELOV1 (**Figure S6A**).

Methylated arginine derived from protein and or histone degradation, and their specific methyltransferases, may regulate MΦ polarization. Dimethylated arginine-glycine (RG/GR) peptides were highly abundant and present in significantly higher quantities in M1- relative to M2-MΦs. Although further confirmation is needed, the data suggests RG/GR-domain-containing proteins such as H4-R3 and RelA (R30), are hypermethylated. Perhaps most importantly, L-NMMA and ADMA are also known to modulate NO production by competing for the arginine binding site of NOS. This creates a potential intersection of arginine metabolism, protein post-translational methylation which is SAM/one-carbon metabolism dependent, protein degradation, and the modulation of NO production.

## Experimental procedures

### M1- and M2-MΦ cell culture, differentiation, isotope tracing, and hypoxia

Human peripheral blood-derived buffy coat of HIV negative and MTB negative healthy donors (male and females, deidentified) were purchased from the Gulf Coast Regional Blood Center/Bank in Houston (1400 La Concha Ln, Houston, TX 77054), which is exempt from IRB regulations of Houston Methodist Research Institute. Blood from about 10 donors was used in this study. All blood samples were processed per approved IRB (HSCA00000993) protocols of the Houston Methodist Research Institute. Procedures and phenotype/purity determination of PBMC-derived and -differentiated macrophages have been previously described (29). Briefly, $CD14^+$ magnetic bead (Miltenyi Inc., USA)-purified monocytes from PBMCs were grown in Iscove's medium (IMDM) with 10% FBS and 10 ng/mL GM-CSF at $4x10^6$ per well in six-well tissue plates for 6 days and then rested for 24 h in GM-CSF-free medium. Cells were differentiated using IFN-γ (10 ng/mL) or IL-4 (10 ng/mL) in GM-CSF-free medium for 48 h to obtain M1- and M2-MΦs, respectively. M0-MΦs were not treated with cytokines. For isotope tracing experiments, M0-, M1-, and M2-MΦs were washed once with PBS and then incubated in RPMI-1460 medium with stable isotope-labeled 2 g/L D-glucose (U-$^{13}C_6$, 99%, Cambridge, Ca#: CLM-1396-1) and 200 µM L-serine (2,3,3-$D_3$,98%, Cambridge, Ca#: DLM-582-0.5) for an additional two and three days, respectively. IFN-γ (10 ng/mL) or IL-4 (10 ng/mL) were

added again for M1- and M2-MΦs. Separated sets of M0-, M1-, and M2-MΦs were cultured and treated simultaneously under hypoxic conditions (2% $O_2$).

**Triomics approach**

Triomics refers to 'metabolomics, proteomics, and OMICs of histone modifications.' We integrated these three OMICs seamlessly in a one-sample preparation followed by an analysis of metabolites, histone modifications, and proteins on the QExactive mass spectrometer (**Figure 1**). Briefly, cell pellets of M0-, M1-, and M2-MΦs were lysed using radioimmunoprecipitation assay (RIPA) buffer (ThermoFisher Scientific, Cat#:89901) supplemented with 1% Nonidet P40, PMSF (0.2 mM), and Roche complete protease inhibitor cocktail (ThermoFisher Scientific, Cat#: 50-100-3301, one tablet per 10 mL lysis buffer). The protein concentrations were measured by Bicinchoninic Acid Assay (BCA). An aliquot (~100 µL) of lysate containing 100 µg proteins was immersed in 500 µL of precooled (-20°C) acetone overnight. After centrifugation, metabolites in the supernatant were submitted for metabolomics analysis, and the proteins in the precipitates were used for the analysis of histone modifications and differential proteins expression.

**Analysis of primary amines including amino acids by dansylation derivatization followed by nanoLC-MS/MS analysis**

Primary amine compounds, including amino acids, were derivatized by dansylation before analysis by nano-LC/MS based on a method (75), (76) and adapted to our nanoLC-QExactive systems. Briefly, 100 µL acetone extraction was mixed with 10 µL internal standards containing 0.1 mM $^{13}C_2$, 2,2-$^{2}H_2$, $^{15}$N-Glycine (Cambridge isotope Lab., Cat#: CDNLM-6799-0.25), 0.1 mM $^{13}C_3$, $^{2}H_3$, $^{15}$N-Serine (Cambridge isotope Lab., Cat#: CDNLM-6813-0.25) and 0.1 mM Methyl-$D_3$-Methionine (Cambridge isotope Lab., Cat#: DLM-431-1), vacuum-dried, and then 30 µL of 0.5M $Na_2CO_3$/$NaHCO_3$ and 100 µL of dansyl chloride (4 mg dissolved in 1 mL acetone) was added and incubated at 55°C for 1 h. After drying under vacuum, dansylated metabolites were dissolved in 50 µL 88% formic acid and 50 µL 1% formic acid. A 20 µL-aliquot was desalted by $C_{18}$ desalting columns. After removal of acetonitrile which was used to elute the dansylated compounds, eluates were dissolved in 50 µL 40% methanol in 1% formic acid. This solution with further diluted 10x with 1% formic acid. 2 µl of this solution was injected each time through the autosampler and analyzed by nanoLC-MS/MS on the QExactive benchtop orbitrap mass spectrometer. The HPLC column was made in-house by packing Magic $C_{18}$-AQ (100 Å, 3 µm, Bruker, Cat#: PM3/61100/00) package material into 20 cm (length) x 360 µm (outer diameter) x75 µm (internal diameter) capillary with PicoTip emitter (New Objective, Cat#: PF360-75-15-N-5) under high pressure. Using this method, amino acids, serine, glycine, and methionine were accurately measured using their stable-isotope labeled compounds as internal standards, and concentrations of other compounds were estimated by mass spectrometry signal normalization against that of either serine in the low retention time zone or glycine in the high retention time zone.

**Analysis of carbonyl-containing compounds including TCA intermediates by O-BHA derivatization followed by nanoLC-MS/MS analysis**

A previously reported method was adapted (77). Acetone extracts (200 µL), with added 10 µL mixture of internal standards containing 0.1 mM each of sodium $D_3$-pyruvate (Cambridge isotope Lab., Cat#: DLM-6068-0), sodium $^{13}C_3$-L-lactate (Cambridge isotope Lab., Cat#: CLM-1579-N-0.1MG), 1,5,6-$^{13}C_3$-citric acid (Cambridge isotope Lab., Cat#: CLM-9876-0.1MG), 1,2,3,4-$^{13}C_4$-α-ketoglutaric acid disodium salt (Cambridge isotope Lab., Cat#: CLM-4442-0.1MG), $^{13}C_4$-succinic acid (Cambridge isotope Lab., Cat#: CLM-1571-0.1MG), $^{13}C_4$-fumaric acid (Cambridge isotope Lab., Cat#: CLM-1529-0.1MG), $^{13}C_4$-L-malic acid

(Cambridge isotope Lab., Cat#: CLM-8065-0.1MG), were completely dried under vacuum. In the dried vials, 50 µL of 1-ethyl-3-(3-dimethylaminopropyl) carbodiimide (EDC), 100 µL of O-benzylhydroxylamine (O-BHA) in pyridine buffer (preparation (200 mL): 15 mL of pyridine (99.8%, Sigma) + 10 mL HCl (12 N) and 175 mL $H_2O$) were added sequentially and then incubated at 30°C for 1 h. After derivatization, metabolites were extracted by 2 x 300 µL ethyl ester. After vacuum drying, 200 µL of 40% methanol was added to dissolve the metabolites. The solution was further diluted 10x with 1% formic acid and submitted for nanoLC-MS/MS analysis on the QExactive. Using this method, carboxylic acids were analyzed. The concentrations of TCA intermediates were accurately measured using their stable isotope-labeled compounds as internal standards, whereas others were estimated by mass spectrometric signal normalization against malate.

**Analysis of histone modifications and the transferring of acetyl-groups from metabolites to histones**

An aliquot of cell lysate containing 20 µg of total proteins was mixed with 1 µg of SILAC-produced heavy arginine ($^{13}C_6{}^{15}N_4$, aka, $^{10}R$) histones (purity > 99%) before being loaded onto SDS-PAGE gel for electrophoresis separation. Gel bands covering molecular weights from 9 to 20 KDa containing histones were cut for in-gel digestion with trypsin. Quantification of histone modifications was carried out by parallel-reaction-monitoring (PRM) on the QExactive instrument using a previously reported inclusion list (78,79). The ratios of MS peak areas of modified peptides over histone peptides without modifications were calculated as the modification percentages used for comparison among M0-, M1-, and M2-MΦ samples. For monitoring methyl- transfer from 3,3,2-$^{2}$H-serine or acetyl- from $^{13}C_6$-glucose to histones, except that no $^{10}R$-histones were added as internal standards. In this case, relative ratios of the ion intensities of isotope-labeled $^{13}C_2$-acetyl-lysine peaks over those of unlabeled peaks were calculated as the isotope incorporation (or transfer) rates.

**Analysis of protein expression**

Cell lysates of each sample containing 50 µg of proteins were reduced by adding 200 µM TCEP (tris(2-carboxyethyl) phosphine) and incubating at 55°C for 1 h, followed by carbamidomethylation of cysteines by adding 375 mM iodoacetamide and incubating the mixture in the dark for 30 minutes. Proteins were precipitated by adding six volumes of precooled acetone and freezing at -20°C overnight and then pelleted at 13,000 rpm for 10 min at 4°C. The protein pellets were then dissolved in 100 mM triethylammonium bicarbonate (TEB) buffer followed by digestion with trypsin/Lyc-C (ThermoFisher Scientific, Cat#: A40007) at a protein/enzyme ratio of 25:1. A tandem mass tag (TMT) labeling kit (TMTsixplex (TMT6)) (ThermoFisher Scientific, Cat#: 90064) was used to label the peptides according to manufacturer instructions. All of the indicated chemicals and solutions were included in this kit unless otherwise specified. M0-, M1-, and M2-MΦ samples were labeled with TMT6 -126 and TMT6-127, TMT6 -128 and TMT6-129, and TMT-130 and TMT-131, respectively. After labeling and quenching, the six samples were desalted by Pierce graphite spin columns (ThermoFisher Scientific, Cat#: 88302) and then mixed. The peptide mixture was fractionated into eight fractions with the Pierce High pH Reversed-Phase Peptide Fractionation Kit (ThermoFisher Scientific, Cat#: 84868) and dried by vacuum centrifugation. Each fraction was resuspended in 25 µL 1% formic acid and analyzed by nanoLC-MS/MS on the QExactive. The same column used for metabolite analysis was used for peptide separation. Reversed-phase liquid chromatography was run for 230 min (solvent A, 0.1% formic acid in water; solvent B, 0.1% formic acid in acetonitrile). A gradient of 5%-45% of solvent B was used for peptide separation. The QExactive was set to acquire data at a resolution of 35,000 in full scan mode and 17,500 in MS/MS mode. The top 15 most intense ions in each MS survey scan were automatically selected for MS/MS. The LC- and MS-running conditions (settings) were very similar for metabolites and peptides.

**Data analysis and statistical analysis**

Each sample was a pool of cell pellets from three wells of a six-well plate ($3x4x10^6$ cells). At least 8 injections of LC-MS/MS were performed for every sample analyzed. Metabolomics data acquired from QExactive instrument were processed by Xcalibur. Metabolite peak areas were integrated after manually inputting the calculated metabolites of interest. Less than 5 ppm between calculated mass and measured mass was considered an authentic identification; however, in most cases, identification was further verified by fragmentation patterns consistent with the molecule's chemical structure. A two-tailed Student's t-test was used to test for the significance of metabolic changes between M1- and M2-MΦ for the volcano plot visualization. Otherwise for all bar graphs shown a one-way ANOVA was used with Dunnett's test for multiple comparisons to the M1-MΦs with GraphPad PRISM. P-values < 0.03 are denoted *, <0.002 **, < 0.0002 ***, < 0.0001 ****.

Histone modifications were evaluated by the percentage (or ratio) of the peak area of a modified peptide over a peptide free of modifications which were normalized to the percentage (or proportion) of the same pair of peptides with stable isotope labeling at arginine (79). Two-tailed Student's t-Test of the Excel-imbedded T.TEST function was used to test for the significance of modification changes between M1- and M2-Mϕ.

Proteins were identified with the Proteome Discoverer (PD) 2.2 platform (version 2.2.0.388, Thermo Fisher Scientific) using the SEQUEST HT search engine that employs the nr_human_062321validated.fasta database with 420779 protein sequence entries *(downloaded on June 23, 2021).* SEQUEST HT parameters were specified as trypsin enzyme, three missed cleavages allowed, minimum peptide length of four, precursor mass tolerance of 10 ppm, and a fragment mass tolerance of 0.02 Da. Oxidation of methionine, acetylation at N-terminal, TMT at lysine, and deamination of asparagine were set as variable modifications. Carbamidomethylation of cysteine and TMT at peptide N-termini was set as a fixed modification. Peptides were filtered for a maximum false discovery rate of 1% (strict). Protein quantification was also through PD 2.2 using the reporter ion ratios of TMT for each set. Reporter ions were quantified from MS2 scans using an integration tolerance of 0.04 Da with the most confident centroid setting. At least one unique peptide with a posterior error probability of <0.05 was accepted for quantification, and proteins were grouped. Differential expression between M1- and M2-Mϕs was done using significance analysis of microarrays with permutation-based multiple test correction in the Perseus software (1.6.12.0) (80). The false detection rate was set to 0.01 (1%), and s0 set to 0.32 (~1.25x fold change cutoff).

Protein interaction networks were built upon the list of proteins in gene names identified by proteomics whose expressions had significant changes using the STRING web-based software. Output coordinates were revisualized by Cytoscape with nodes colored from blue (negative $Log_2$ fold change) to red (positive $Log_2$ fold change) based on protein quantification data. Pathways corresponding to a group of proteins selected from proteomics data meeting defined criteria were identified by g:Profiler and visualized by Cytoscape with EnrichmentMap APP (50).

**DATA AVAILABILITY STATEMENT**

Data supporting the original contributions presented in the study are included in the article and supplementary materials. Proteomics raw data and searching results were deposited in ProteomeXchange with the identifier PXD030701.

**ETHICS STATEMENT**

Human blood samples were collected as per approved Institutional Biosafety Committee protocols. The samples were deidentified.

**AUTHOR CONTRIBUTIONS**

MLS, HT, VKS, AK and AM conducted experiments and acquired data; BIR provided reagents. KZ and MLS designed and analyzed data. CJ designed experiments and edited the manuscript.

**ACKNOWLEDGEMENTS**

The authors wish to acknowledge funding support from NIH RO1 AI-122070 (CJ), AI-161015 and HMRI for support funds. We also wish to thank Ellie Cherryhomes for suggestions on scientific communication and proofreading. Several figures were prepared in part with Biorender.

**REFERENCES**


1. Gordon, S., and Pluddemann, A. (2017) Tissue macrophages: heterogeneity and functions. *BMC Biol* **15**, 53
2. Gessain, G., Bleriot, C., and Ginhoux, F. (2020) Non-genetic Heterogeneity of Macrophages in Diseases-A Medical Perspective. *Front Cell Dev Biol* **8**, 613116
3. Grosjean, A., Venteclef, N., and Dalmas, E. (2021) Understanding the heterogeneity and functions of metabolic tissue macrophages. *Semin Cell Dev Biol* **119**, 130-139
4. Zhang, X., and Mosser, D. M. (2008) Macrophage activation by endogenous danger signals. *J Pathol* **214**, 161-178
5. Mills, C. D., Kincaid, K., Alt, J. M., Heilman, M. J., and Hill, A. M. (2000) M-1/M-2 macrophages and the Th1/Th2 paradigm. *J Immunol* **164**, 6166-6173
6. Italiani, P., and Boraschi, D. (2014) From Monocytes to M1/M2 Macrophages: Phenotypical vs. Functional Differentiation. *Front Immunol* **5**, 514
7. Mantovani, A., Sica, A., Sozzani, S., Allavena, P., Vecchi, A., and Locati, M. (2004) The chemokine system in diverse forms of macrophage activation and polarization. *Trends Immunol* **25**, 677-686
8. Wang, N., Liang, H., and Zen, K. (2014) Molecular mechanisms that influence the macrophage m1-m2 polarization balance. *Front Immunol* **5**, 614
9. Chinetti-Gbaguidi, G., and Staels, B. (2011) Macrophage polarization in metabolic disorders: functions and regulation. *Curr Opin Lipidol* **22**, 365-372
10. Thapa, B., and Lee, K. (2019) Metabolic influence on macrophage polarization and pathogenesis. *BMB Rep* **52**, 360-372
11. Viola, A., Munari, F., Sanchez-Rodriguez, R., Scolaro, T., and Castegna, A. (2019) The Metabolic Signature of Macrophage Responses. *Front Immunol* **10**, 1462
12. Navegantes, K. C., de Souza Gomes, R., Pereira, P. A. T., Czaikoski, P. G., Azevedo, C. H. M., and Monteiro, M. C. (2017) Immune modulation of some autoimmune diseases: the critical role of macrophages and neutrophils in the innate and adaptive immunity. *J Transl Med* **15**, 36
13. Saradna, A., Do, D. C., Kumar, S., Fu, Q. L., and Gao, P. (2018) Macrophage polarization and allergic asthma. *Transl Res* **191**, 1-14
14. Najafi, M., Hashemi Goradel, N., Farhood, B., Salehi, E., Nashtaei, M. S., Khanlarkhani, N., Khezri, Z., Majidpoor, J., Abouzaripour, M., Habibi, M., Kashani, I. R., and Mortezaee, K. (2019) Macrophage polarity in cancer: A review. *J Cell Biochem* **120**, 2756-2765
15. Baardman, J., Licht, I., de Winther, M. P., and Van den Bossche, J. (2015) Metabolic-epigenetic crosstalk in macrophage activation. *Epigenomics* **7**, 1155-1164
16. Noe, J. T., Rendon, B. E., Geller, A. E., Conroy, L. R., Morrissey, S. M., Young, L. E. A., Bruntz, R. C., Kim, E. J., Wise-Mitchell, A., Barbosa de Souza Rizzo, M., Relich, E. R., Baby, B. V., Johnson, L. A., Affronti, H. C., McMasters, K. M., Clem, B. F., Gentry, M. S., Yan, J., Wellen, K. E., Sun, R. C., and Mitchell, R. A. (2021) Lactate supports a metabolic-epigenetic link in macrophage polarization. *Sci Adv* **7**, eabi8602
17. Francesca De Santa, L. V., Alessio Torcinaro, and Elisabetta Ferraro. (2019) The Role of Metabolic Remodeling in Macrophage Polarization and Its Effect on Skeletal Muscle Regeneration *Antioxidants and Redox Signaling* **30**, 1553-1598
18. Galvan-Pena, S., and O'Neill, L. A. (2014) Metabolic reprograming in macrophage polarization. *Front Immunol* **5**, 420
19. Jha, A. K., Huang, S. C., Sergushichev, A., Lampropoulou, V., Ivanova, Y., Loginicheva, E., Chmielewski, K., Stewart, K. M., Ashall, J., Everts, B., Pearce, E. J., Driggers, E. M., and Artyomov, M. N. (2015) Network integration of parallel metabolic and transcriptional data reveals metabolic modules that regulate macrophage polarization. *Immunity* **42**, 419-430

20. Martinez, F. O., Gordon, S., Locati, M., and Mantovani, A. (2006) Transcriptional profiling of the human monocyte-to-macrophage differentiation and polarization: new molecules and patterns of gene expression. *J Immunol* **177**, 7303-7311
21. Wink, D. A., Hines, H. B., Cheng, R. Y., Switzer, C. H., Flores-Santana, W., Vitek, M. P., Ridnour, L. A., and Colton, C. A. (2011) Nitric oxide and redox mechanisms in the immune response. *J Leukoc Biol* **89**, 873-891
22. Nagy, C., and Haschemi, A. (2015) Time and Demand are Two Critical Dimensions of Immunometabolism: The Process of Macrophage Activation and the Pentose Phosphate Pathway. *Front Immunol* **6**, 164
23. James, M. J., Gibson, R. A., and Cleland, L. G. (2000) Dietary polyunsaturated fatty acids and inflammatory mediator production. *Am J Clin Nutr* **71**, 343S-348S
24. Cuevas, A., Saavedra, N., Salazar, L. A., and Abdalla, D. S. (2013) Modulation of immune function by polyphenols: possible contribution of epigenetic factors. *Nutrients* **5**, 2314-2332
25. Pepe, G., Braga, D., Renzi, T. A., Villa, A., Bolego, C., D'Avila, F., Barlassina, C., Maggi, A., Locati, M., and Vegeto, E. (2017) Self-renewal and phenotypic conversion are the main physiological responses of macrophages to the endogenous estrogen surge. *Sci Rep* **7**, 44270
26. Dall'Asta, M., Derlindati, E., Ardigo, D., Zavaroni, I., Brighenti, F., and Del Rio, D. (2012) Macrophage polarization: the answer to the diet/inflammation conundrum? *Nutr Metab Cardiovasc Dis* **22**, 387-392
27. Orillion, A., Damayanti, N. P., Shen, L., Adelaiye-Ogala, R., Affronti, H., Elbanna, M., Chintala, S., Ciesielski, M., Fontana, L., Kao, C., Elzey, B. D., Ratliff, T. L., Nelson, D. E., Smiraglia, D., Abrams, S. I., and Pili, R. (2018) Dietary Protein Restriction Reprograms Tumor-Associated Macrophages and Enhances Immunotherapy. *Clin Cancer Res* **24**, 6383-6395
28. Dos Santos, L. M., da Silva, T. M., Azambuja, J. H., Ramos, P. T., Oliveira, P. S., da Silveira, E. F., Pedra, N. S., Galdino, K., do Couto, C. A., Soares, M. S., Tavares, R. G., Spanevello, R. M., Stefanello, F. M., and Braganhol, E. (2017) Methionine and methionine sulfoxide treatment induces M1/classical macrophage polarization and modulates oxidative stress and purinergic signaling parameters. *Mol Cell Biochem* **424**, 69-78
29. Henze, A. T., and Mazzone, M. (2016) The impact of hypoxia on tumor-associated macrophages. *J Clin Invest* **126**, 3672-3679
30. Rabhi, N., Hannou, S. A., Froguel, P., and Annicotte, J. S. (2017) Cofactors As Metabolic Sensors Driving Cell Adaptation in Physiology and Disease. *Front Endocrinol (Lausanne)* **8**, 304
31. Kaelin, W. G., Jr., and McKnight, S. L. (2013) Influence of metabolism on epigenetics and disease. *Cell* **153**, 56-69
32. Cai, L., Sutter, B. M., Li, B., and Tu, B. P. (2011) Acetyl-CoA induces cell growth and proliferation by promoting the acetylation of histones at growth genes. *Mol Cell* **42**, 426-437
33. Cluntun, A. A., Huang, H., Dai, L., Liu, X., Zhao, Y., and Locasale, J. W. (2015) The rate of glycolysis quantitatively mediates specific histone acetylation sites. *Cancer Metab* **3**, 10
34. Shen, F., Boccuto, L., Pauly, R., Srikanth, S., and Chandrasekaran, S. (2019) Genome-scale network model of metabolism and histone acetylation reveals metabolic dependencies of histone deacetylase inhibitors. *Genome Biol* **20**, 49
35. Wellen, K. E., Hatzivassiliou, G., Sachdeva, U. M., Bui, T. V., Cross, J. R., and Thompson, C. B. (2009) ATP-citrate lyase links cellular metabolism to histone acetylation. *Science* **324**, 1076-1080
36. Yucel, N., Wang, Y. X., Mai, T., Porpiglia, E., Lund, P. J., Markov, G., Garcia, B. A., Bendall, S. C., Angelo, M., and Blau, H. M. (2019) Glucose Metabolism Drives Histone Acetylation Landscape Transitions that Dictate Muscle Stem Cell Function. *Cell Rep* **27**, 3939-3955 e3936

37. Kamphorst, J. J., Chung, M. K., Fan, J., and Rabinowitz, J. D. (2014) Quantitative analysis of acetyl-CoA production in hypoxic cancer cells reveals substantial contribution from acetate. *Cancer Metab* **2**, 23
38. Chiang, T. T., Hung, C. T., Wang, W. M., Lee, J. T., and Yang, F. C. (2013) Recreational nitrous oxide abuse-induced vitamin B12 deficiency in a patient presenting with hyperpigmentation of the skin. *Case Rep Dermatol* **5**, 186-191
39. Hadzic, A., Glab, K., Sanborn, K. V., and Thys, D. M. (1995) Severe neurologic deficit after nitrous oxide anesthesia. *Anesthesiology* **83**, 863-866
40. Stockton, L., Simonsen, C., and Seago, S. (2017) Nitrous oxide-induced vitamin B12 deficiency. *Proc (Bayl Univ Med Cent)* **30**, 171-172
41. Sharma, V. S., Pilz, R. B., Boss, G. R., and Magde, D. (2003) Reactions of nitric oxide with vitamin B12 and its precursor, cobinamide. *Biochemistry* **42**, 8900-8908
42. Meiser, J., Kramer, L., Sapcariu, S. C., Battello, N., Ghelfi, J., D'Herouel, A. F., Skupin, A., and Hiller, K. (2016) Pro-inflammatory Macrophages Sustain Pyruvate Oxidation through Pyruvate Dehydrogenase for the Synthesis of Itaconate and to Enable Cytokine Expression. *J Biol Chem* **291**, 3932-3946
43. Shen, H., Campanello, G. C., Flicker, D., Grabarek, Z., Hu, J., Luo, C., Banerjee, R., and Mootha, V. K. (2017) The Human Knockout Gene CLYBL Connects Itaconate to Vitamin B12. *Cell* **171**, 771-782 e711
44. Zhang, K., Xu, P., Sowers, J. L., Machuca, D. F., Mirfattah, B., Herring, J., Tang, H., Chen, Y., Tian, B., Brasier, A. R., and Sowers, L. C. (2017) Proteome Analysis of Hypoxic Glioblastoma Cells Reveals Sequential Metabolic Adaptation of One-Carbon Metabolic Pathways. *Mol Cell Proteomics* **16**, 1906-1921
45. Samaniego, R., Palacios, B. S., Domiguez-Soto, A., Vidal, C., Salas, A., Matsuyama, T., Sanchez-Torres, C., de la Torre, I., Miranda-Carus, M. E., Sanchez-Mateos, P., and Puig-Kroger, A. (2014) Macrophage uptake and accumulation of folates are polarization-dependent in vitro and in vivo and are regulated by activin A. *J Leukoc Biol* **95**, 797-808
46. Tang, H., Tian, B., Brasier, A. R., Sowers, L. C., and Zhang, K. (2016) Measurement of Histone Methylation Dynamics by One-Carbon Metabolic Isotope Labeling and High-energy Collisional Dissociation Methylation Signature Ion Detection. *Sci Rep* **6**, 31537
47. Khan, A., Zhang, K., Singh, V. K., Mishra, A., Kachroo, P., Bing, T., Won, J. H., Mani, A., Papanna, R., Mann, L. K., Ledezma-Campos, E., Aguillon-Duran, G., Canaday, D. H., David, S. A., Restrepo, B. I., Viet, N. N., Phan, H., Graviss, E. A., Musser, J. M., Kaushal, D., Gauduin, M. C., and Jagannath, C. (2022) Human M1 macrophages express unique innate immune response genes after mycobacterial infection to defend against tuberculosis. *Commun Biol* **5**, 480
48. Weng, I. C., Chen, H. L., Lo, T. H., Lin, W. H., Chen, H. Y., Hsu, D. K., and Liu, F. T. (2018) Cytosolic galectin-3 and -8 regulate antibacterial autophagy through differential recognition of host glycans on damaged phagosomes. *Glycobiology* **28**, 392-405
49. Rothgiesser, K. M., Erener, S., Waibel, S., Lüscher, B., and Hottiger, M. O. (2010) SIRT2 regulates NF-κB dependent gene expression through deacetylation of p65 Lys310. *J Cell Sci* **123**, 4251-4258
50. Reimand, J., Isserlin, R., Voisin, V., Kucera, M., Tannus-Lopes, C., Rostamianfar, A., Wadi, L., Meyer, M., Wong, J., Xu, C., Merico, D., and Bader, G. D. (2019) Pathway enrichment analysis and visualization of omics data using g:Profiler, GSEA, Cytoscape and EnrichmentMap. *Nat Protoc* **14**, 482-517
51. Kazak, L., and Cohen, P. (2020) Creatine metabolism: energy homeostasis, immunity and cancer biology. *Nat Rev Endocrinol* **16**, 421-436

52. Sastre, M., Galea, E., Feinstein, D., Reis, D. J., and Regunathan, S. (1998) Metabolism of agmatine in macrophages: modulation by lipopolysaccharide and inhibitory cytokines. *Biochem J* **330 ( Pt 3)**, 1405-1409
53. Hartel, N. G., Liu, C. Z., and Graham, N. A. (2020) Improved Discrimination of Asymmetric and Symmetric Arginine Dimethylation by Optimization of the Normalized Collision Energy in Liquid Chromatography-Mass Spectrometry Proteomics. *J Proteome Res* **19**, 3123-3129
54. Leiper, J., and Vallance, P. (1999) Biological significance of endogenous methylarginines that inhibit nitric oxide synthases. *Cardiovasc Res* **43**, 542-548
55. Blanc, R. S., and Richard, S. (2017) Arginine Methylation: The Coming of Age. *Mol Cell* **65**, 8-24
56. Sun, Q., Liu, L., Roth, M., Tian, J., He, Q., Zhong, B., Bao, R., Lan, X., Jiang, C., Sun, J., Yang, X., and Lu, S. (2015) PRMT1 Upregulated by Epithelial Proinflammatory Cytokines Participates in COX2 Expression in Fibroblasts and Chronic Antigen-Induced Pulmonary Inflammation. *J Immunol* **195**, 298-306
57. Kim, J. H., Yoo, B. C., Yang, W. S., Kim, E., Hong, S., and Cho, J. Y. (2016) The Role of Protein Arginine Methyltransferases in Inflammatory Responses. *Mediators Inflamm* **2016**, 4028353
58. Harris, D. P., Bandyopadhyay, S., Maxwell, T. J., Willard, B., and DiCorleto, P. E. (2014) Tumor necrosis factor (TNF)-α induction of CXCL10 in endothelial cells requires protein arginine methyltransferase 5 (PRMT5)-mediated nuclear factor (NF)-κB p65 methylation. *J Biol Chem* **289**, 15328-15339
59. Schmidt, S. K., Ebel, S., Keil, E., Woite, C., Ernst, J. F., Benzin, A. E., Rupp, J., and Daubener, W. (2013) Regulation of IDO activity by oxygen supply: inhibitory effects on antimicrobial and immunoregulatory functions. *PLoS One* **8**, e63301
60. Nino-Castro, A., Abdullah, Z., Popov, A., Thabet, Y., Beyer, M., Knolle, P., Domann, E., Chakraborty, T., Schmidt, S. V., and Schultze, J. L. (2014) The IDO1-induced kynurenines play a major role in the antimicrobial effect of human myeloid cells against Listeria monocytogenes. *Innate Immun* **20**, 401-411
61. Kuhn, D. M., and Arthur, R. E., Jr. (1996) Inactivation of brain tryptophan hydroxylase by nitric oxide. *J Neurochem* **67**, 1072-1077
62. Herr, N., Bode, C., and Duerschmied, D. (2017) The Effects of Serotonin in Immune Cells. *Front Cardiovasc Med* **4**, 48
63. Sternberg, E. M., Wedner, H. J., Leung, M. K., and Parker, C. W. (1987) Effect of serotonin (5-HT) and other monoamines on murine macrophages: modulation of interferon-gamma induced phagocytosis. *J Immunol* **138**, 4360-4365
64. Domínguez-Soto, Á., Usategui, A., Casas-Engel, M. L., Simón-Fuentes, M., Nieto, C., Cuevas, V. D., Vega, M. A., Luis Pablos, J., and Corbí, Á. (2017) Serotonin drives the acquisition of a profibrotic and anti-inflammatory gene profile through the 5-HT7R-PKA signaling axis. *Sci Rep* **7**, 14761
65. Aldajani, W. A., Salazar, F., Sewell, H. F., Knox, A., and Ghaemmaghami, A. M. (2016) Expression and regulation of immune-modulatory enzyme indoleamine 2,3-dioxygenase (IDO) by human airway epithelial cells and its effect on T cell activation. *Oncotarget* **7**, 57606-57617
66. Frazão, J. B., Thain, A., Zhu, Z., Luengo, M., Condino-Neto, A., and Newburger, P. E. (2015) Regulation of CYBB Gene Expression in Human Phagocytes by a Distant Upstream NF-κB Binding Site. *J Cell Biochem* **116**, 2008-2017
67. Palmieri, E. M., Gonzalez-Cotto, M., Baseler, W. A., Davies, L. C., Ghesquiere, B., Maio, N., Rice, C. M., Rouault, T. A., Cassel, T., Higashi, R. M., Lane, A. N., Fan, T. W., Wink, D. A., and McVicar, D. W. (2020) Nitric oxide orchestrates metabolic rewiring in M1 macrophages by targeting aconitase 2 and pyruvate dehydrogenase. *Nat Commun* **11**, 698
68. Langston, P. K., Shibata, M., and Horng, T. (2017) Metabolism Supports Macrophage Activation. *Front Immunol* **8**, 61

69. Huber, K., Hofer, D. C., Trefely, S., Pelzmann, H. J., Madreiter-Sokolowski, C., Duta-Mare, M., Schlager, S., Trausinger, G., Stryeck, S., Graier, W. F., Kolb, D., Magnes, C., Snyder, N. W., Prokesch, A., Kratky, D., Madl, T., Wellen, K. E., and Bogner-Strauss, J. G. (2019) N-acetylaspartate pathway is nutrient responsive and coordinates lipid and energy metabolism in brown adipocytes. *Biochim Biophys Acta Mol Cell Res* **1866**, 337-348
70. Bogner-Strauss, J. G. (2017) -Acetylaspartate Metabolism Outside the Brain: Lipogenesis, Histone Acetylation, and Cancer. *Front Endocrinol (Lausanne)* **8**, 240
71. Prokesch, A., Pelzmann, H. J., Pessentheiner, A. R., Huber, K., Madreiter-Sokolowski, C. T., Drougard, A., Schittmayer, M., Kolb, D., Magnes, C., Trausinger, G., Graier, W. F., Birner-Gruenberger, R., Pospisilik, J. A., and Bogner-Strauss, J. G. (2016) N-acetylaspartate catabolism determines cytosolic acetyl-CoA levels and histone acetylation in brown adipocytes. *Sci Rep* **6**, 23723
72. Zyśk, M., Sakowicz-Burkiewicz, M., Pikul, P., Kowalski, R., Michno, A., and Pawełczyk, T. (2020) The Impact of Acetyl-CoA and Aspartate Shortages on the N-Acetylaspartate Level in Different Models of Cholinergic Neurons. *Antioxidants (Basel)* **9**
73. Morizono, H., Cabrera-Luque, J., Shi, D., Gallegos, R., Yamaguchi, S., Yu, X., Allewell, N. M., Malamy, M. H., and Tuchman, M. (2006) Acetylornithine transcarbamylase: a novel enzyme in arginine biosynthesis. *J Bacteriol* **188**, 2974-2982
74. Kim, J. W., Tchernyshyov, I., Semenza, G. L., and Dang, C. V. (2006) HIF-1-mediated expression of pyruvate dehydrogenase kinase: a metabolic switch required for cellular adaptation to hypoxia. *Cell Metab* **3**, 177-185
75. Li, Z., Tatlay, J., and Li, L. (2015) Nanoflow LC-MS for High-Performance Chemical Isotope Labeling Quantitative Metabolomics. *Anal Chem* **87**, 11468-11474
76. Guo, K., and Li, L. (2009) Differential 12C-/13C-isotope dansylation labeling and fast liquid chromatography/mass spectrometry for absolute and relative quantification of the metabolome. *Anal Chem* **81**, 3919-3932
77. Tan, B., Lu, Z., Dong, S., Zhao, G., and Kuo, M. S. (2014) Derivatization of the tricarboxylic acid intermediates with O-benzylhydroxylamine for liquid chromatography-tandem mass spectrometry detection. *Anal Biochem* **465**, 134-147
78. Tang, H., Fang, H., Yin, E., Brasier, A. R., Sowers, L. C., and Zhang, K. (2014) Multiplexed parallel reaction monitoring targeting histone modifications on the QExactive mass spectrometer. *Anal Chem* **86**, 5526-5534
79. Sowers, J. L., Mirfattah, B., Xu, P., Tang, H., Park, I. Y., Walker, C., Wu, P., Laezza, F., Sowers, L. C., and Zhang, K. (2015) Quantification of histone modifications by parallel-reaction monitoring: a method validation. *Anal Chem* **87**, 10006-10014
80. Tyanova, S., Temu, T., Sinitcyn, P., Carlson, A., Hein, M. Y., Geiger, T., Mann, M., and Cox, J. (2016) The Perseus computational platform for comprehensive analysis of (prote)omics data. *Nat Methods* **13**, 731-740

**Figure 1. Workflow for triomics for analysis of metabolites, histone modifications (epigenetics), and protein expression (phenotype).**

Cell lysates of M0-, M1- and M2-macrophages (MΦs) are immersed into acetone for extraction of metabolites (supernatants) and proteins (precipitates). A portion of metabolite extract is derivatized by dansylation to analyze primary amines and another portion is derivatized by O-BHA to analyze carboxyl acids by nanoLC-MS/MS. Proteins are resolved by SDS-PAGE and gel bands containing histones (MW < 20K) are cut for in-gel digestion and histone modifications are analyzed by nanoLC-MS/MS using Parallel Reaction Monitoring. Proteins are in-solution digested by trypsin/Lys-C. Peptides are labeled by TMT6plex. TMT6-labeled peptides are analyzed by nanoLC-MS/MS to determine protein expression changed and perturbated protein pathways.

**Figure 2. Alteration of metabolites, histone acetylation and methylation, and protein expression in M1- and M2-Mϕs.**

A. Volcano plot of the fold change in metabolites of M1- versus M2-MΦs. The x-axis is the $\log_2$ of fold changes and the y-axis is the significance of the change of each corresponding metabolite with $\log_{10}$ (p-value) calculated by Student's two-way t-test from at least eight consecutive LC-MS/MS runs. Two separate sample preparation and analysis, and in each preparation of cells from three wells of six-well plates were combined.
B. Volcano plot of the fold change in histone acetylation and methylation in M1- versus M2-MΦs. The plot also includes methylation of arginine, lysine amino acids or two-amino-acid peptides, acetylation of aspartate (NAA), glutamate (NAG), and ornithine (NAO). Data were acquired from the same sample preparation as in A. Biological and technical replicates, and statistical analyses are also the same as in A.
C. Volcano plot of the fold change of proteins in M1- versus M2-MΦs. Protein quantification was performed with one of the two sample preparations and one additional technical replicate was applied by labeling each sample (M0-, M1-, and M2-MΦs) with two TMT tags. Significance of fold changes was tested by microarrays permutation with Perseus software based on FDR set to 0.01 (1%) and s0 set to 0.32 (~1.25x fold change cutoff).
D. Heatmap analysis of up and downregulated proteins in M2-MΦ compared to M1-MΦ and both relative to M0-MΦ.

**Figure 3. Enriched protein pathways in M1-Mϕ and M2-Mϕ.**

A. Enriched pathways built from upregulated proteins in M1-MΦs.
B. Enriched pathways built from upregulated proteins in M2-MΦs.

**Figure 4. Arginine metabolism and methylation in M1-Mϕ vs.M2-Mϕ**

A. Concentrations of arginine pathway metabolites in M0-, M1-, and M2-MΦs measured by LC-MS. Concentrations were calculated by normalizing the signal intensity relative to an internal standard of known concentration, 3,3,2-$^{2}$H-serine.
B. Arginine pathway showing metabolites framed in red or green colors indicating an increase in either M1-MΦ or M2-MΦ. PMRT: Protein Arginine Methyltransferase, ADC: Arginine decarboxylase, AGAT: Arginine:Glycine Amidinotransferase, ASL: Argininosuccinate Lyase, ASS: Argininosuccinate Synthase, OAT: Ornithine Aminotransferase, OTC: Ornithine Transcarbamylase.
C. Heat map showing differential levels of arginine methylation in M0-, M1-, and M2-MΦs.

**Figure 5. Tryptophan metabolism in M1-Mϕ vs.M2-Mϕs.**

A. Concentrations of tryptophan pathway metabolites in M0-, M1-, and M2-MΦs measured by LC-MS. Concentrations were calculated by normalizing the signals of targeting compounds against the signal of 10 µL of 0.1 mM $^{13}C_2$, 2,2-$^{2}H_2$, $^{15}$N-Glycine spiked in 200 µL of acetone extracts.
B. Tryptophan pathway showing metabolites framed in red or green colors indicating an increase in either M1-MΦs or M2. IDO: indoleamine 2,3-dioxygenase, TPH: tryptophan hydroxylase, KMO: kynurenine 3-monooxygenase, KYNU: kynureninase, QPRT: quinolinate phosphoribosyltransferase.
C. Heat map of the expressions of proteins identified in the tryptophan pathway.

**Figure 6. Protein and metabolite alteration in glycolysis, TCA cycle, mitochondria respiration, and aspartate/glutamate to pyruvate shunting pathways in M1-Mϕ vs.M2-Mϕs.**

A. STRING network of proteins detected by quantitative proteomics in glycolysis pathway. Red color: proteins are upregulated in M2-MΦ; blue color: proteins are upregulated in M1-MΦ. $LOG_2$ (Fold changes) of protein expressions (M2-MΦ/ M1-MΦ) are represented by the color key on the bottom.
B. STRING network of proteins detected by quantitative proteomics in mitochondria respiratory chains.
C. STRING network of proteins detected by quantitative proteomics in TCA cycle, pyruvate, and aspartate/glutamate pathways.
D. Concentrations of asparagine, aspartic acid, glutamine, glutamic acid, acetylated aspartic acid, acetylated glutamic acid, acetylated ornithine measured by LC/MS.
E. Heatmap of D.

**Figure 7. Glucose tracing into key metabolites and histone acetylation**

A. $^{13}C_3$-enrichment of pyruvate and lactate and $^{13}C_2$-enrichment of succinate from $^{13}C_6$-glucose metabolism.
B. Percentage of $^{13}C_2$-acetyl enrichment of histone H3K18/K23 after MΦs incubated with $^{13}C_6$-glucose for 48 h under normoxic and hypoxic conditions.
C. Diagram of $^{13}$C enrichment on glycolic and the TCA cycle metabolites and histone acetylation derived from $^{13}C_6$-glucose in M1-Mϕ.

**SUPPLEMENTAL FIGURES**

**Figure S1**. Histone acetylation and methylation in M0-, M1-, and M2-MΦs quantified by parallel-reaction-monitoring (PRM).

**Figure S2.** Concentrations of TCA cycle metabolites and N-acetyl-aspartate, -glutamate, and -ornithine measured by LC-MS/MS.

**Figure S3.** MS/MS spectrum of N-alpha-acetyl-ornithine dansylated derivative.

**Figure S4**: Measurement of methyl and acetyl transfer from metabolites to histones.

Rate of transferring of $^{13}C_6$-glucose to histones: intensity of peak at *m/z* 128.0981 (the immonium ion of $^{13}C_2$-acetylated lysine) over intensity of peak at *m/z* 126.0914 (the immonium ion of acetylated lysine). Shown is a selective MS/MS spectrum of K9me1K14ac.

**Figure S5. Altered one-carbon metabolism and histone methylation in M1- and M2-Mϕs.**

A. A network built up from one carbon metabolism (folate cycle and methionine cycle) proteins quantified by proteomics. Red color: Upregulated in M2-MΦ; Blue color: upregulated in M1-MΦ. Color key is the same for B.
B. Heat map of the relative expression (M2/M1) of the networked proteins.
C. The concentration ratio of methionine (Met) over homocysteine (Hcy) in M0-, M1-, and M2-MΦs.
D. The concentration ratio of S-adenosyl-L-methionine (SAM) over S-adenosyl-homocysteine (SAH) in M0-, M1-, and M2-MΦs.
E. Isotope tracing methyl transfer from 3,3,2-$^{2}$H-serine to methionine (Met) and histone K9 mono- (H3K9me1) and tri-methylation (H3K9me3).
F. A scheme showing the isotope $^{2}$H transferring from serine to histones through the one-carbon pathway that is inhibited by NO.

**Figure S6**. Fatty acid metabolism and oxidation.

A. Networks built upon proteins quantified by proteomics in metabolic pathways of fatty acid oxidation and elongation, as well as production and detoxification of oxidative species. Red color: upregulated in M2-MΦs. Blue color: upregulated in M1-MΦs.
B. Concentrations (nmol/mg protein) of fatty acids and oxidized products in M0-, M1-, and M2-MΦs. 4-HNE: 4-hydroxynonenal; AAAS: aminoadipic acid semialdehyde; AKBA: amino-ketobutyric acid.
C. Heat map showing the changes of the concentrations of fatty acids and oxidized products in B.
D. Networks built upon proteins quantified by proteomics in metabolic pathways of fatty acid oxidation and elongation, as well as production and detoxification of oxidative species. Red color: upregulated in M1-MΦs. Blue color: upregulated in M0-MΦs.

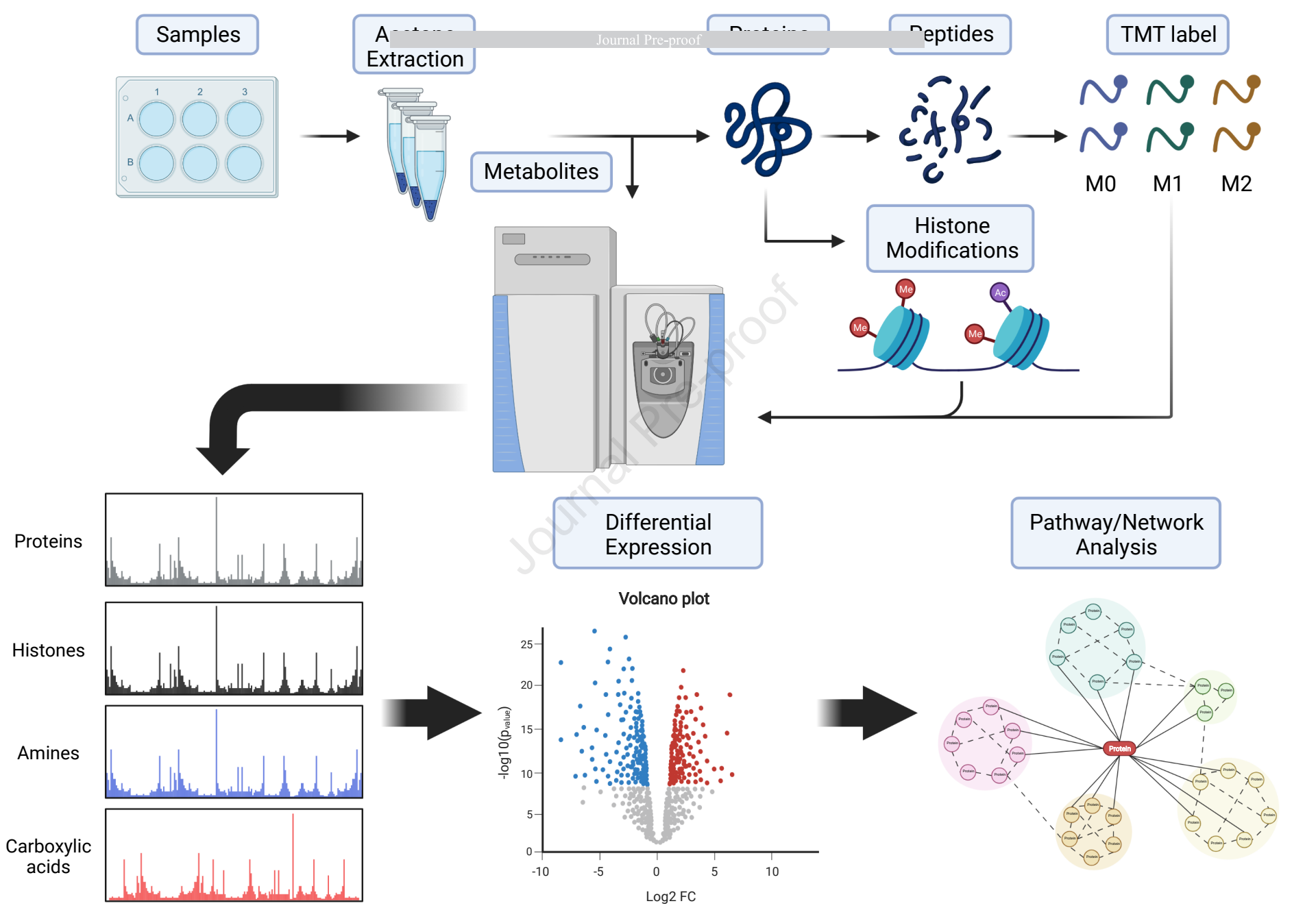

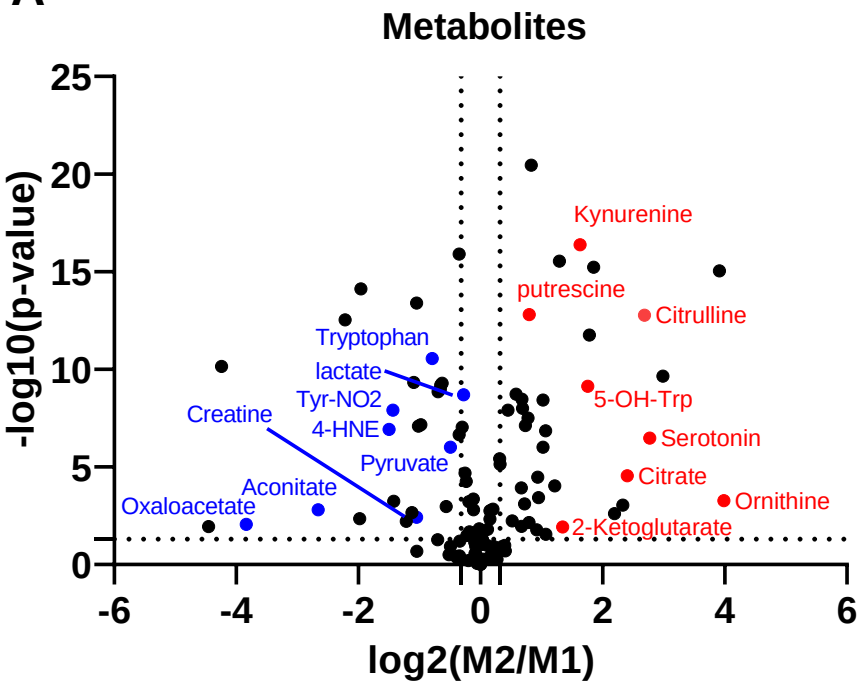


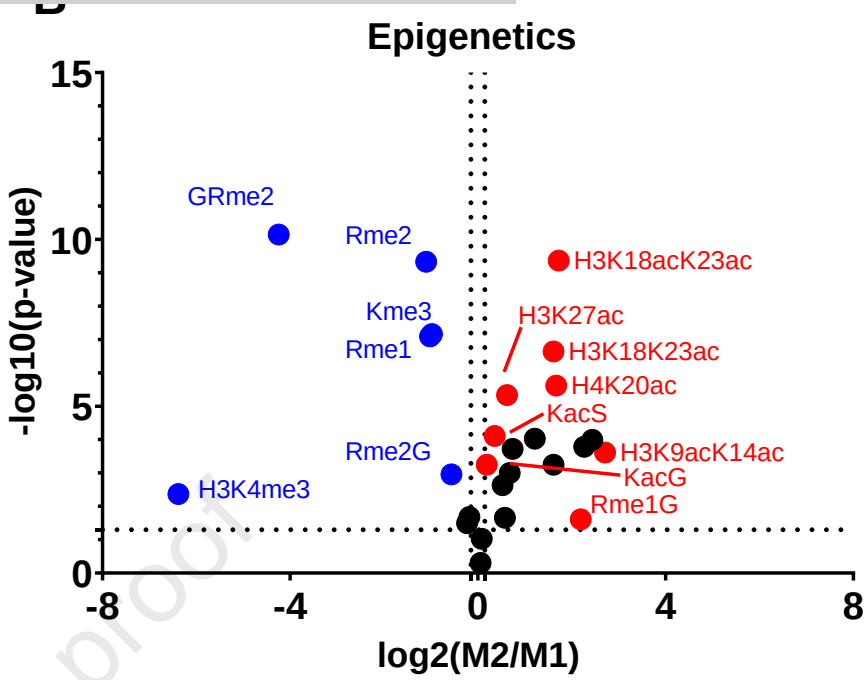


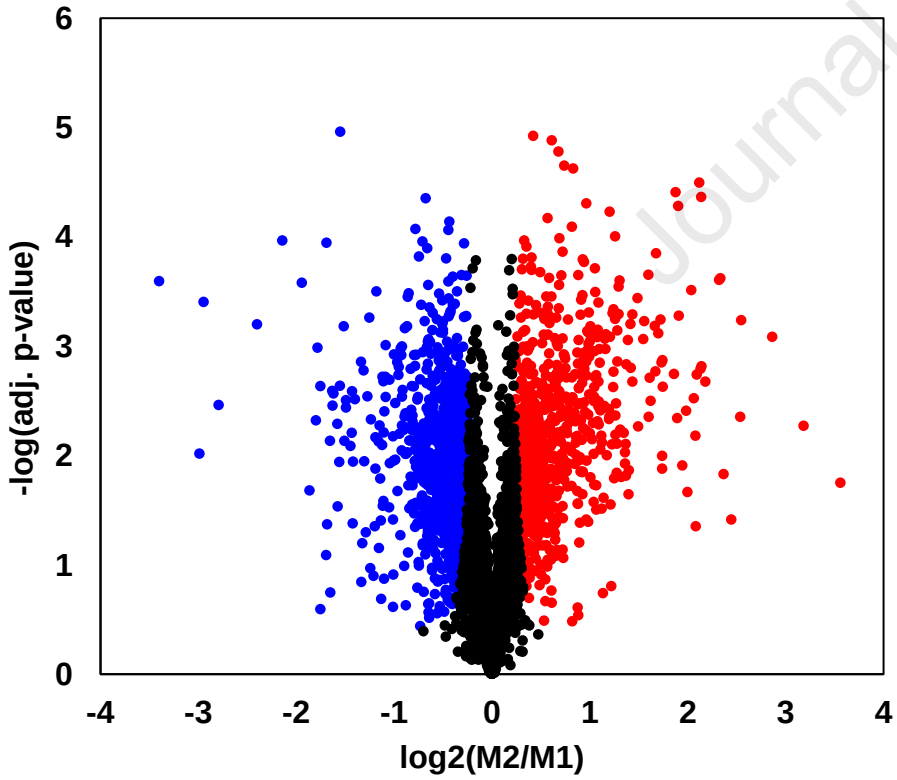


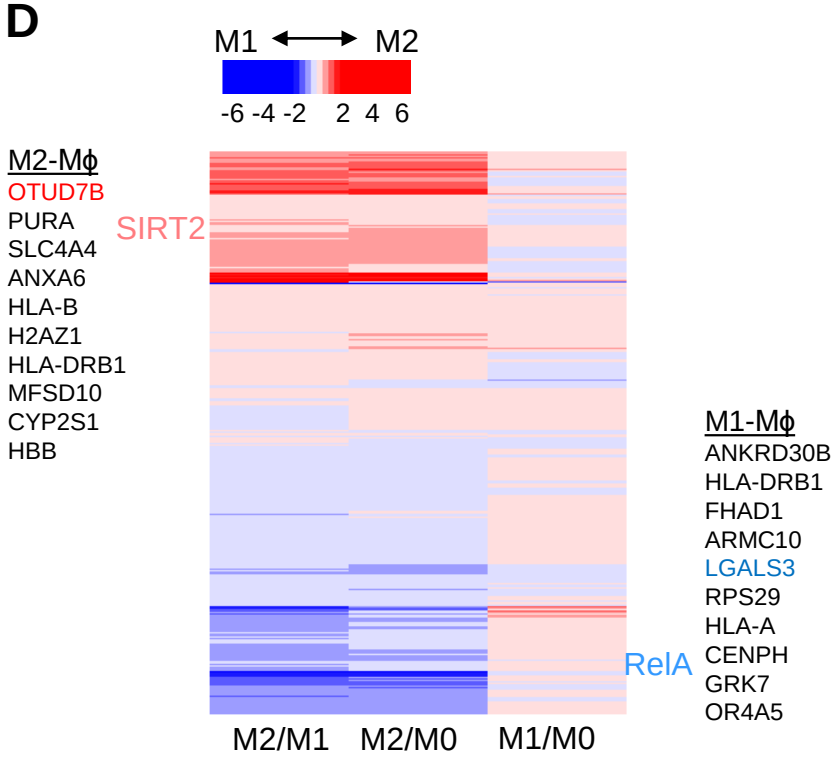

A

## Pathways Enriched in M1-Mϕ

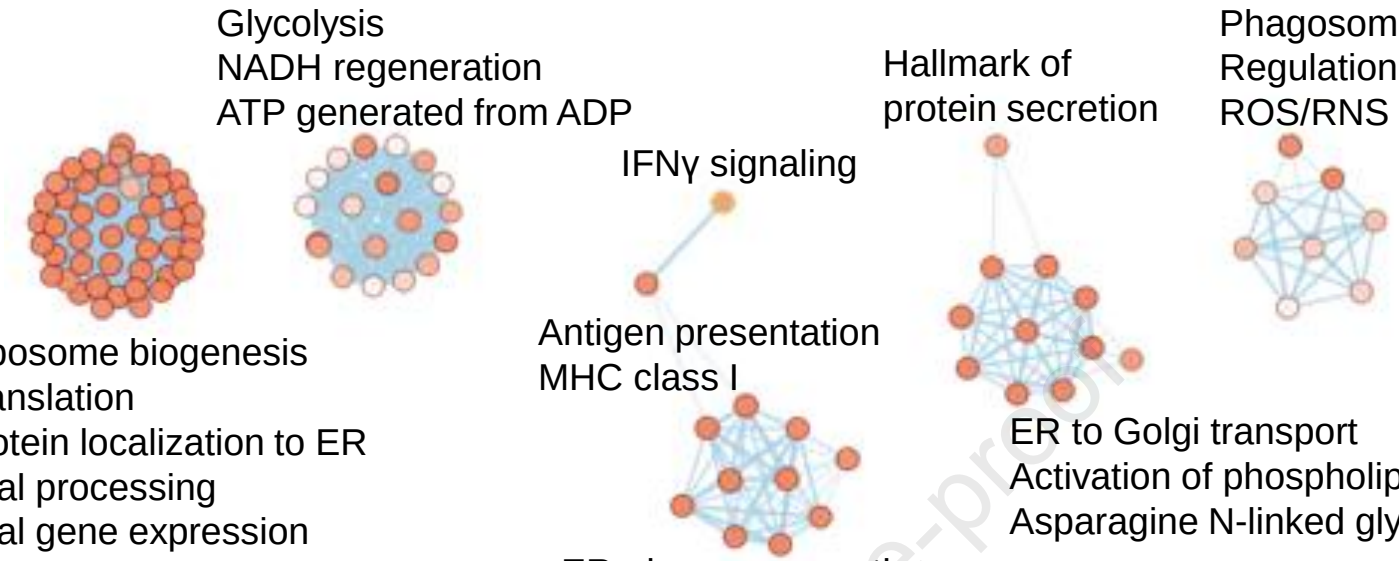


B

## Pathways Enriched in M2-Mϕ

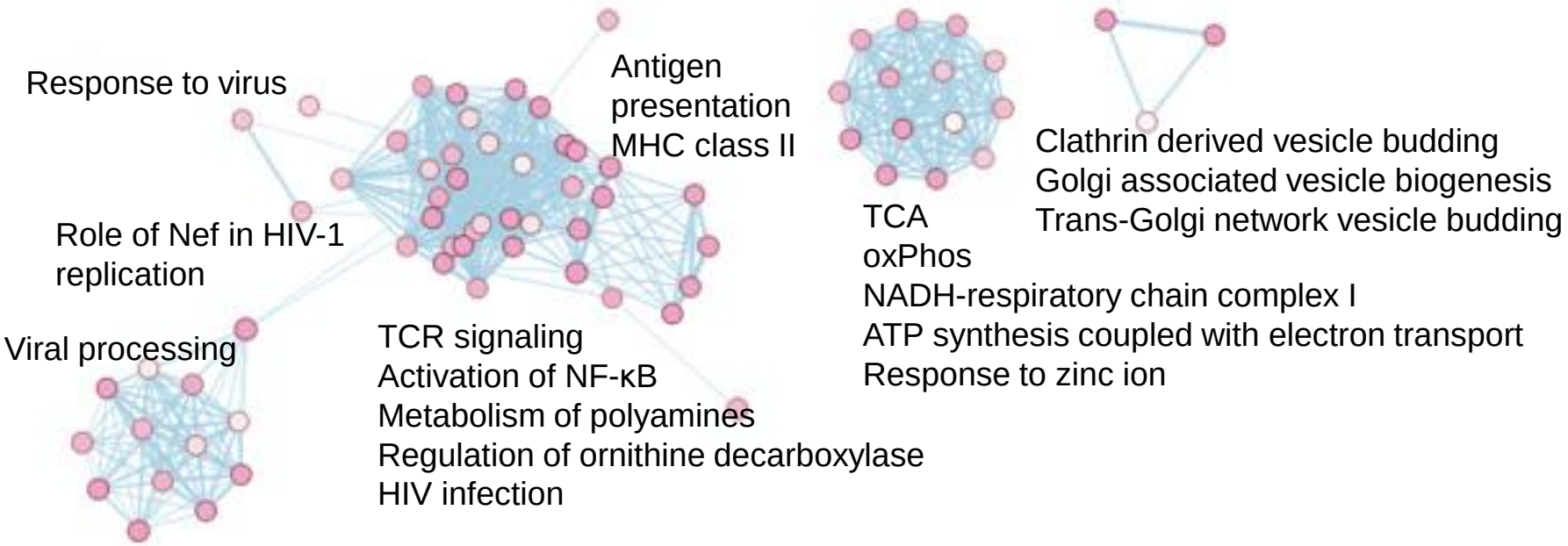

A

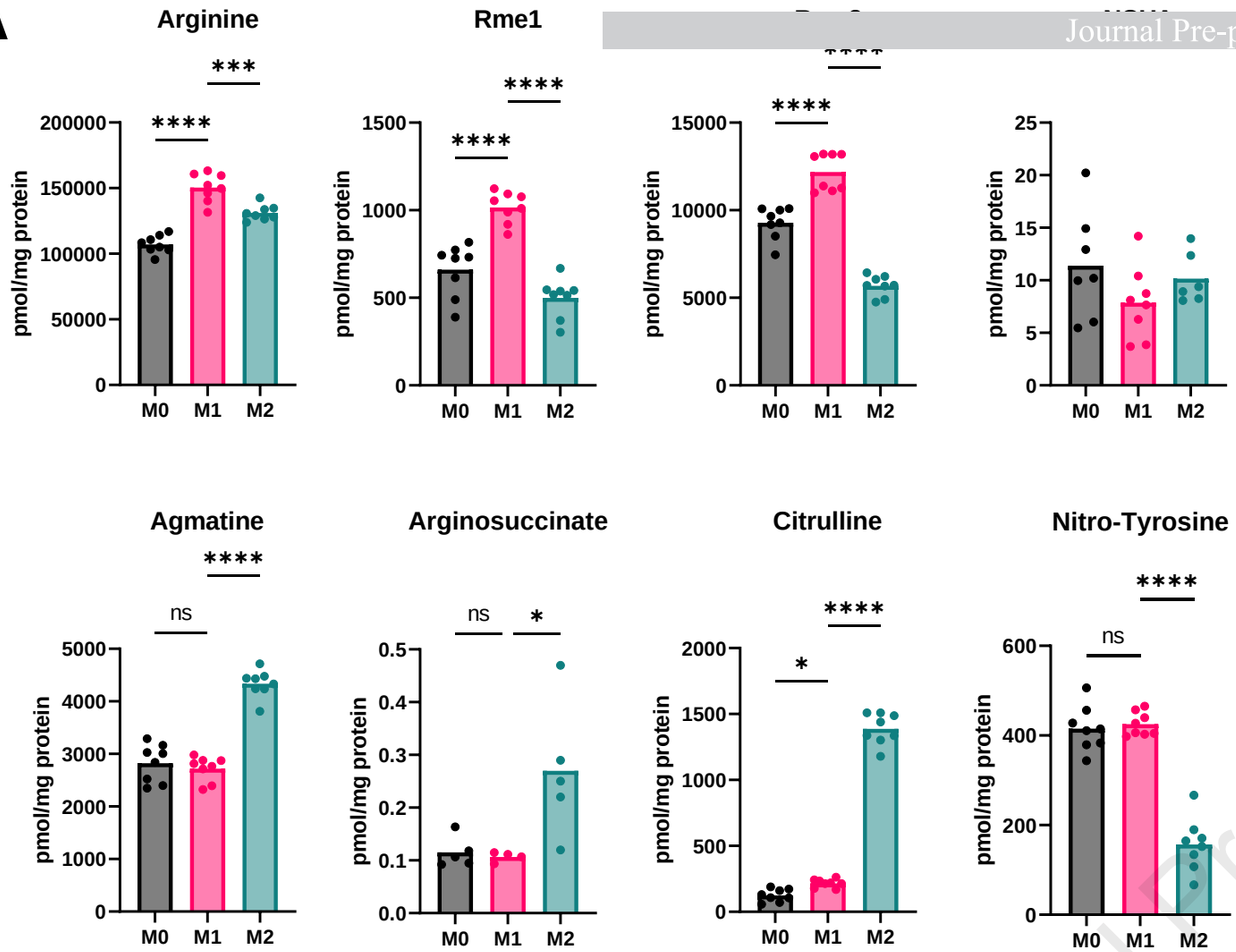


B

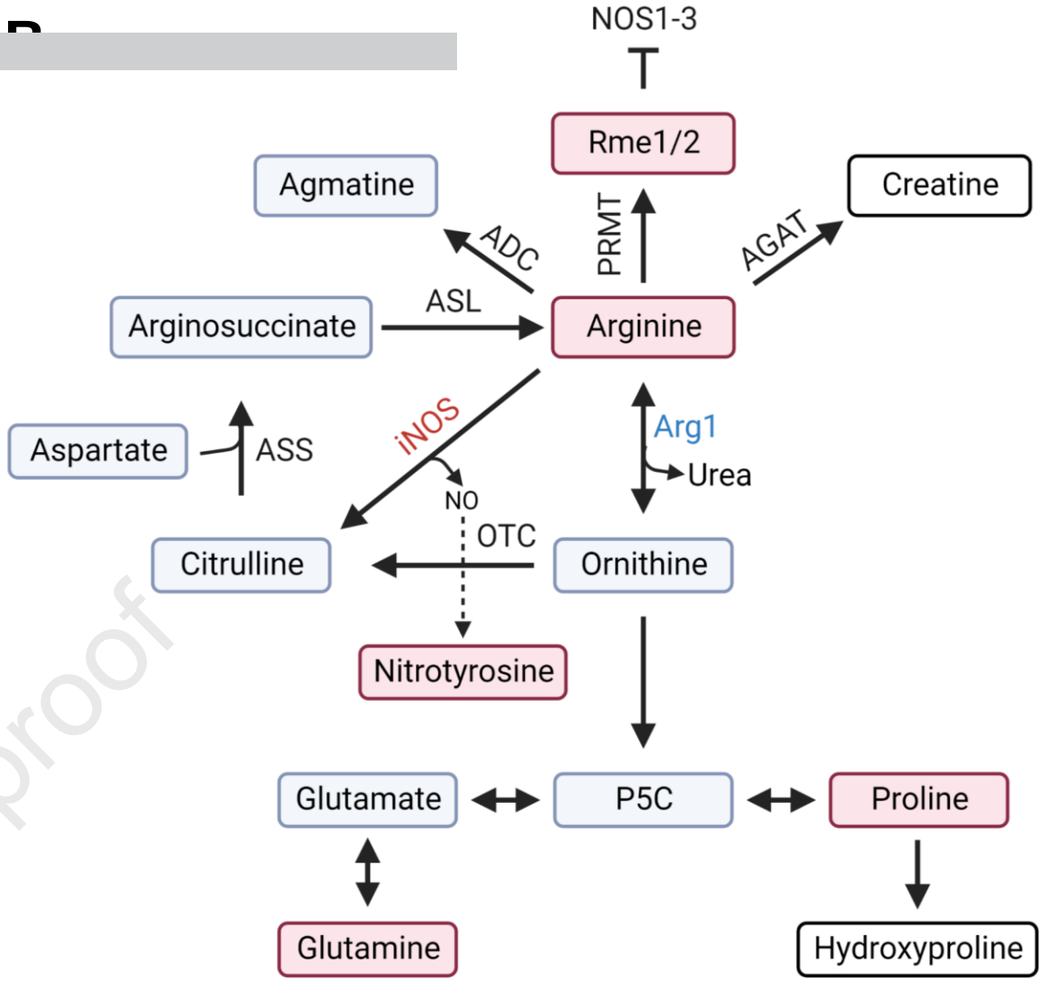


C

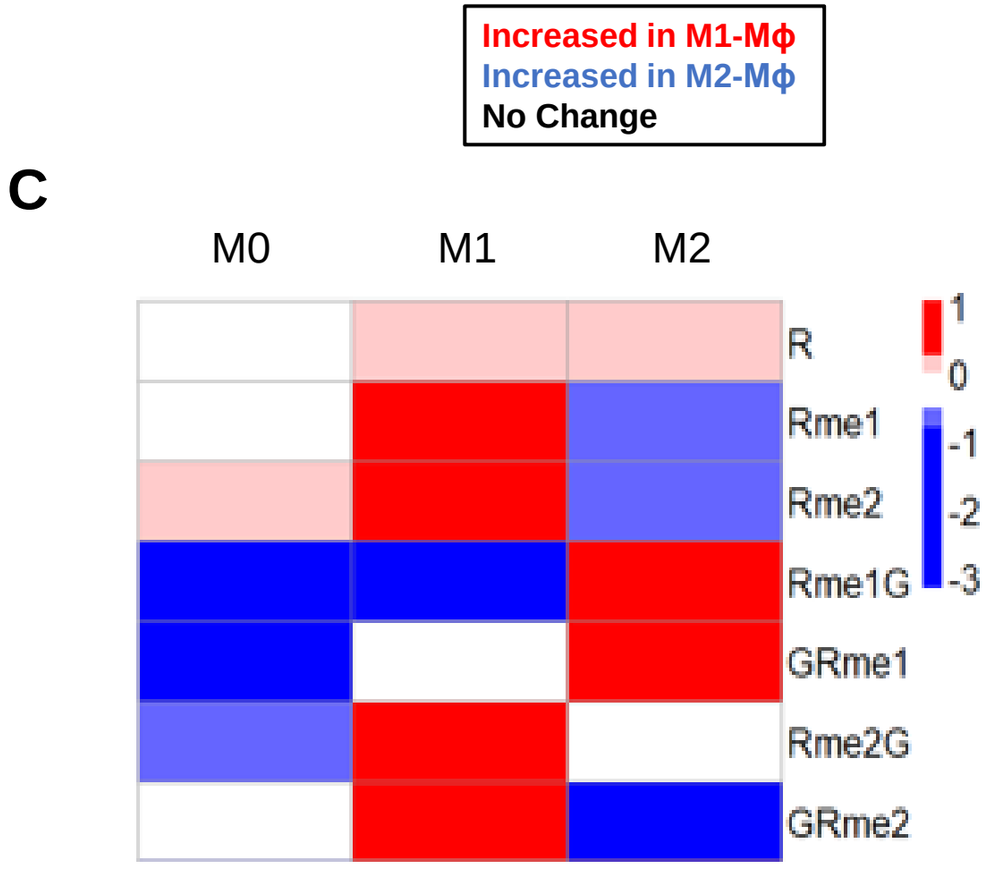

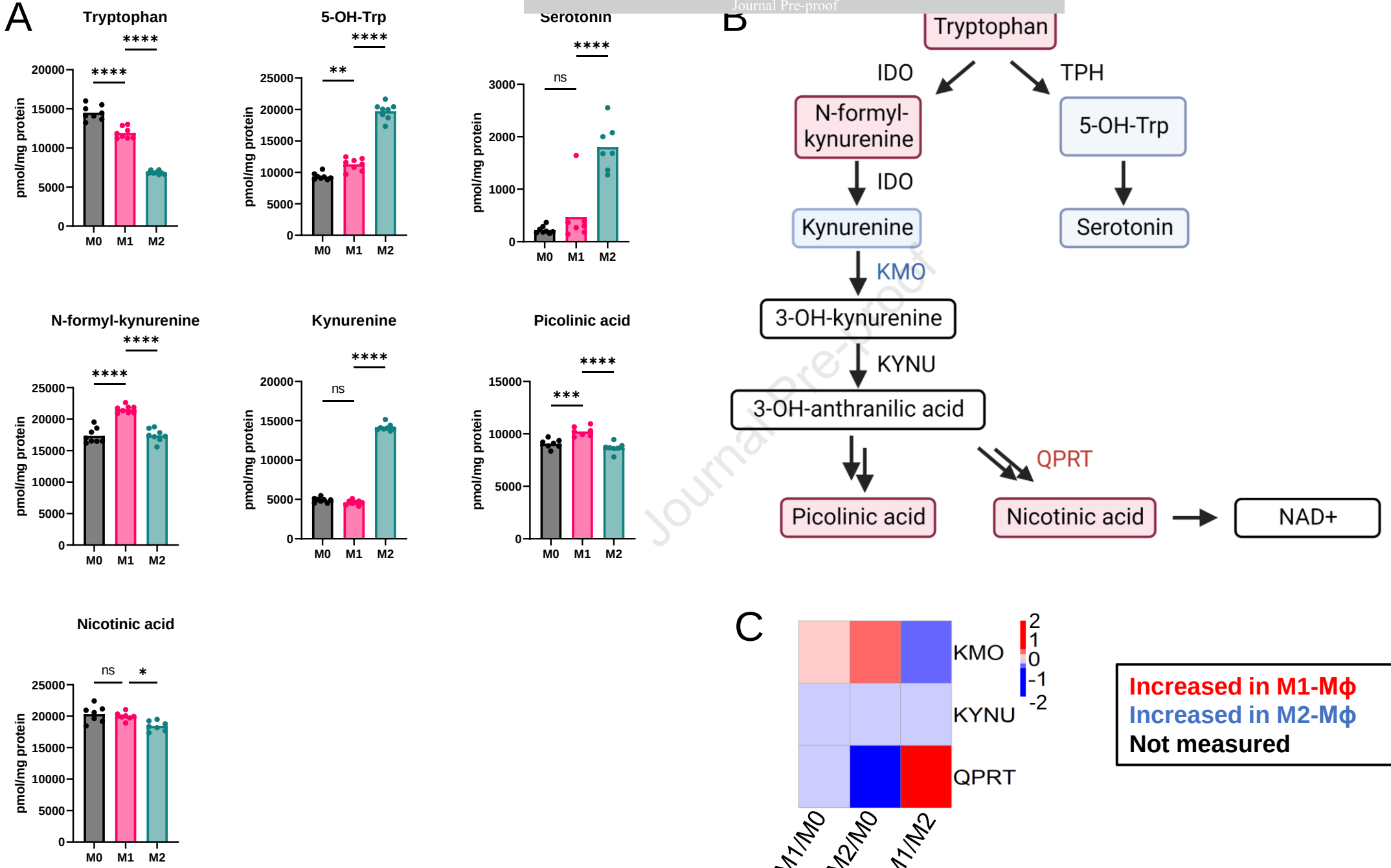

A

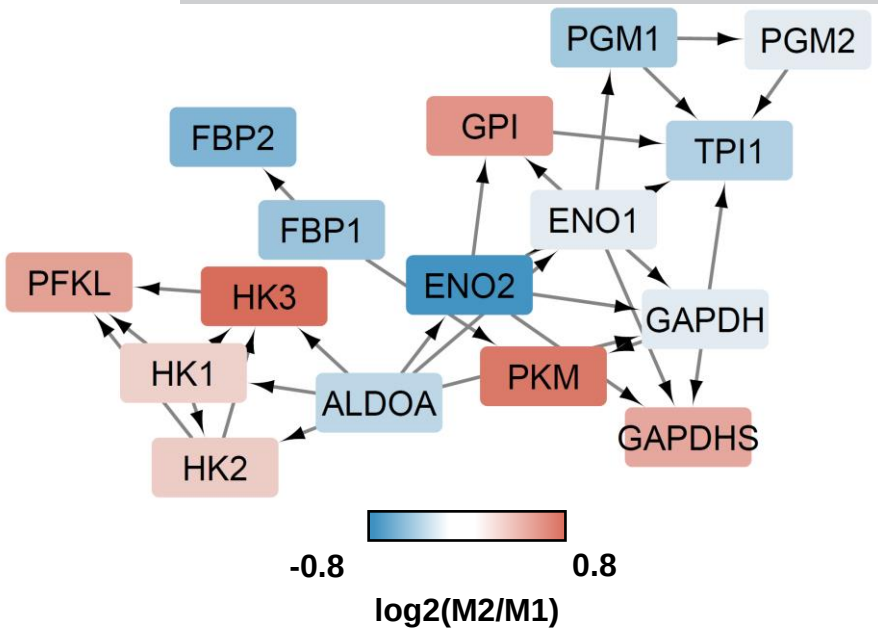


Concentration of amino acids (nmol/mg protein)

| Name | M0-Mϕ | M1-Mϕ | M2-Mϕ | P-value (M1/M2) |
|---|---|---|---|---|
| Asn | 1.024 | 1.287 | 2.607 | 3.77xE-9 |
| Asp | 0.558 | 0.743 | 2.677 | 5.97E-6 |
| NAA | 0.198 | 0.371 | 0.170 | 2.18E-3 |
| Gln | 1.633 | 2.940 | 1.809 | 1.40E-9 |
| Glu | 186.3 | 375.1 | 479.8 | 1.64E-7 |
| NAG | 0.036 | 0.036 | 0.028 | 6.34E-2 |
| NAO | 2.415 | 4.250 | 1.090 | 7.55E-15 |

B

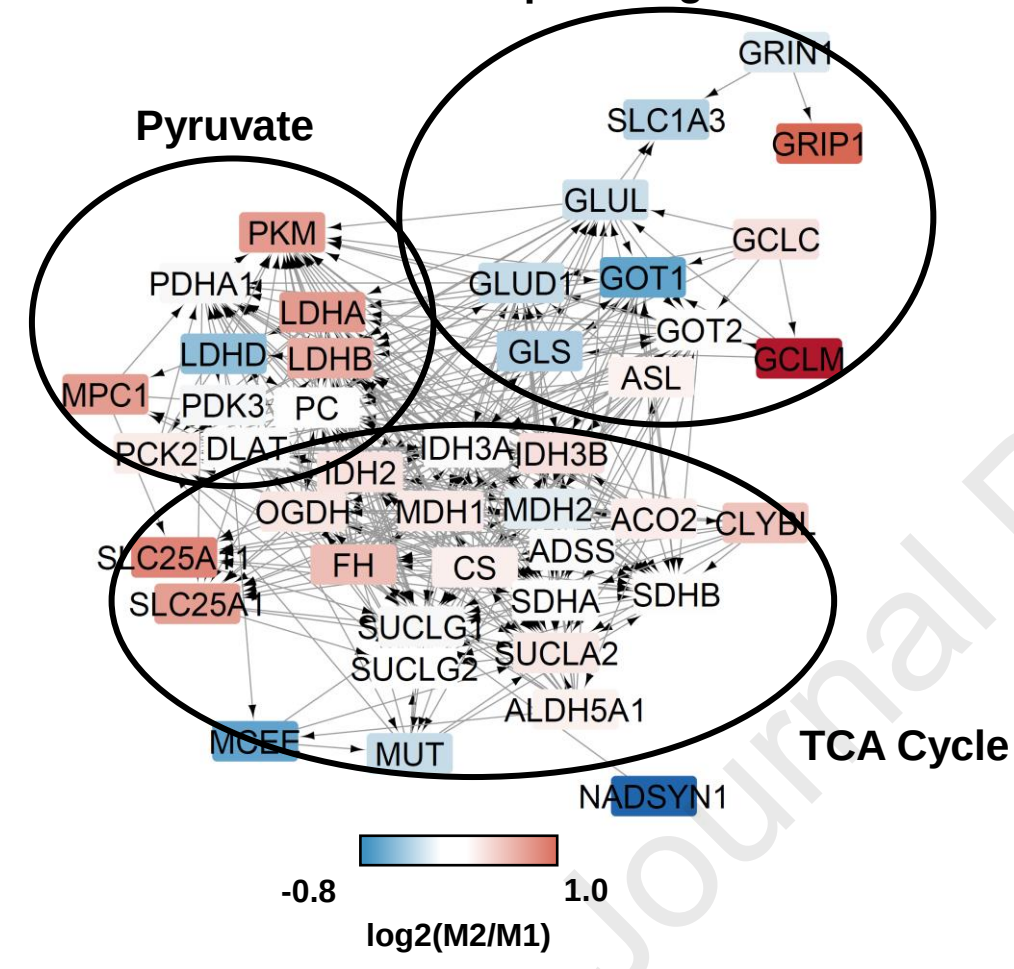


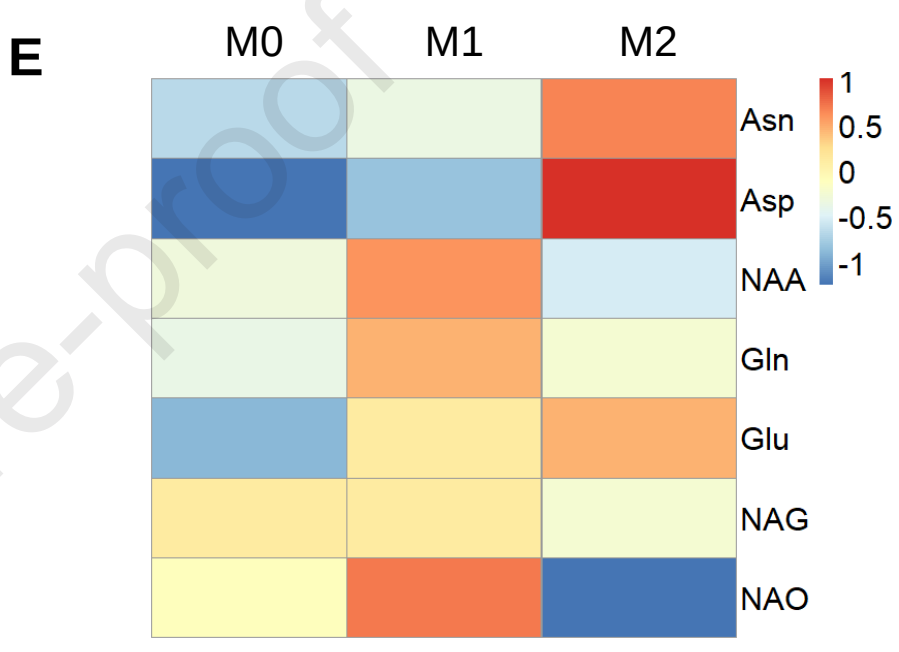


Oxidative Phosphorylation/Mitochondrial Respiration

C

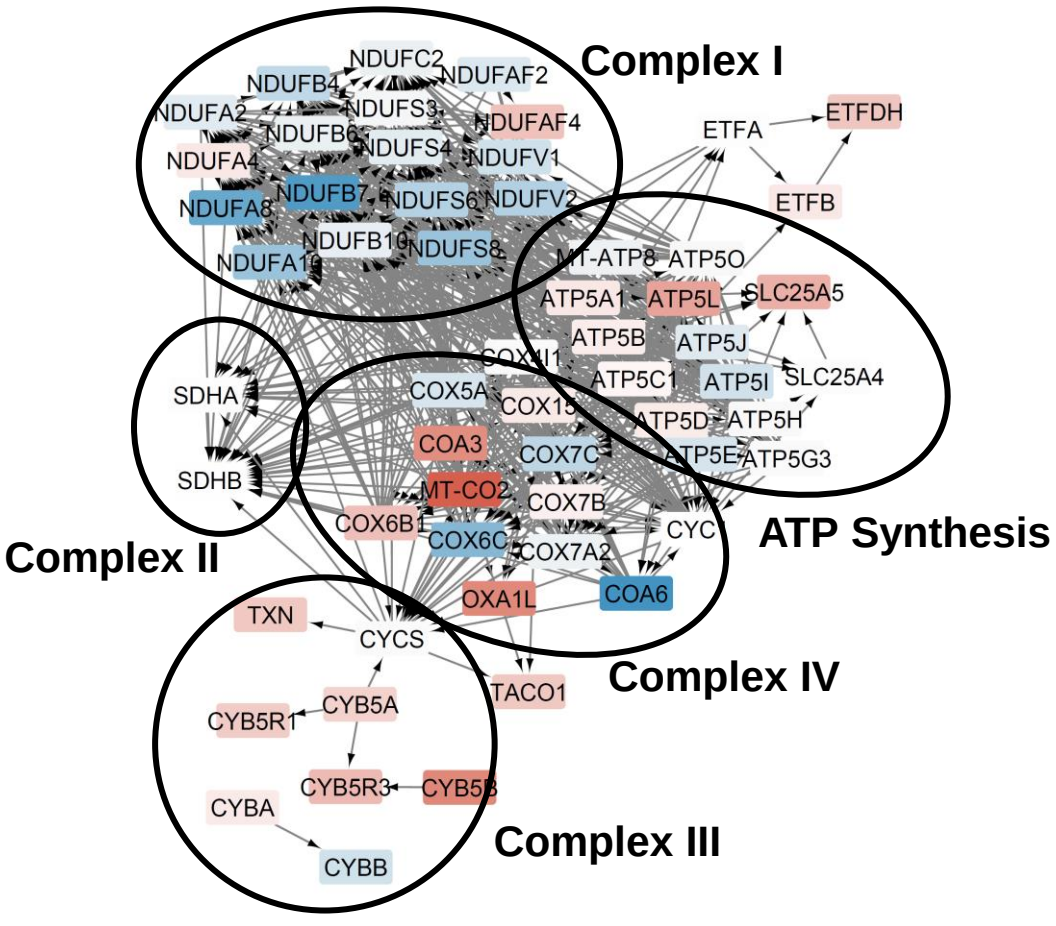

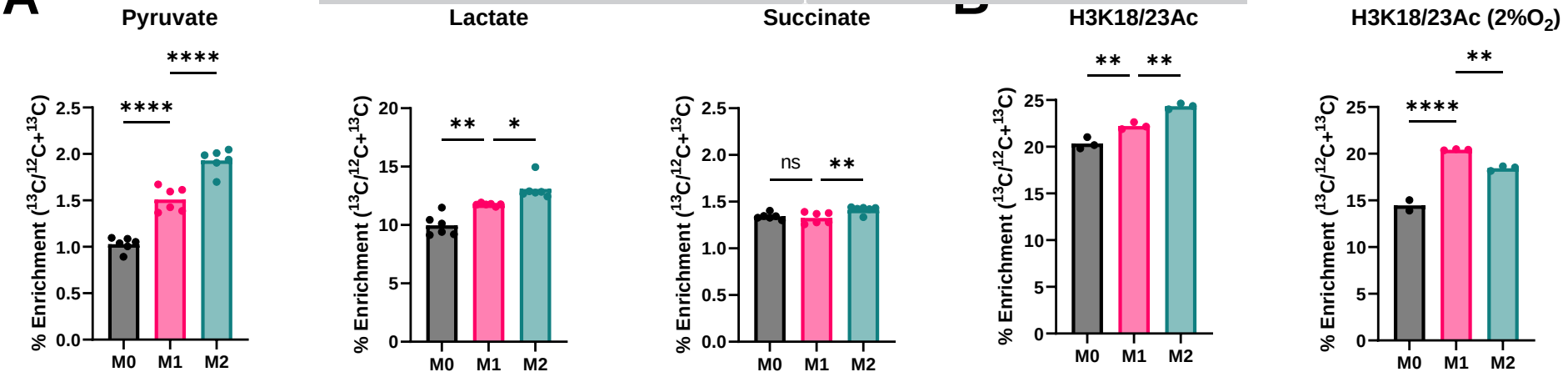


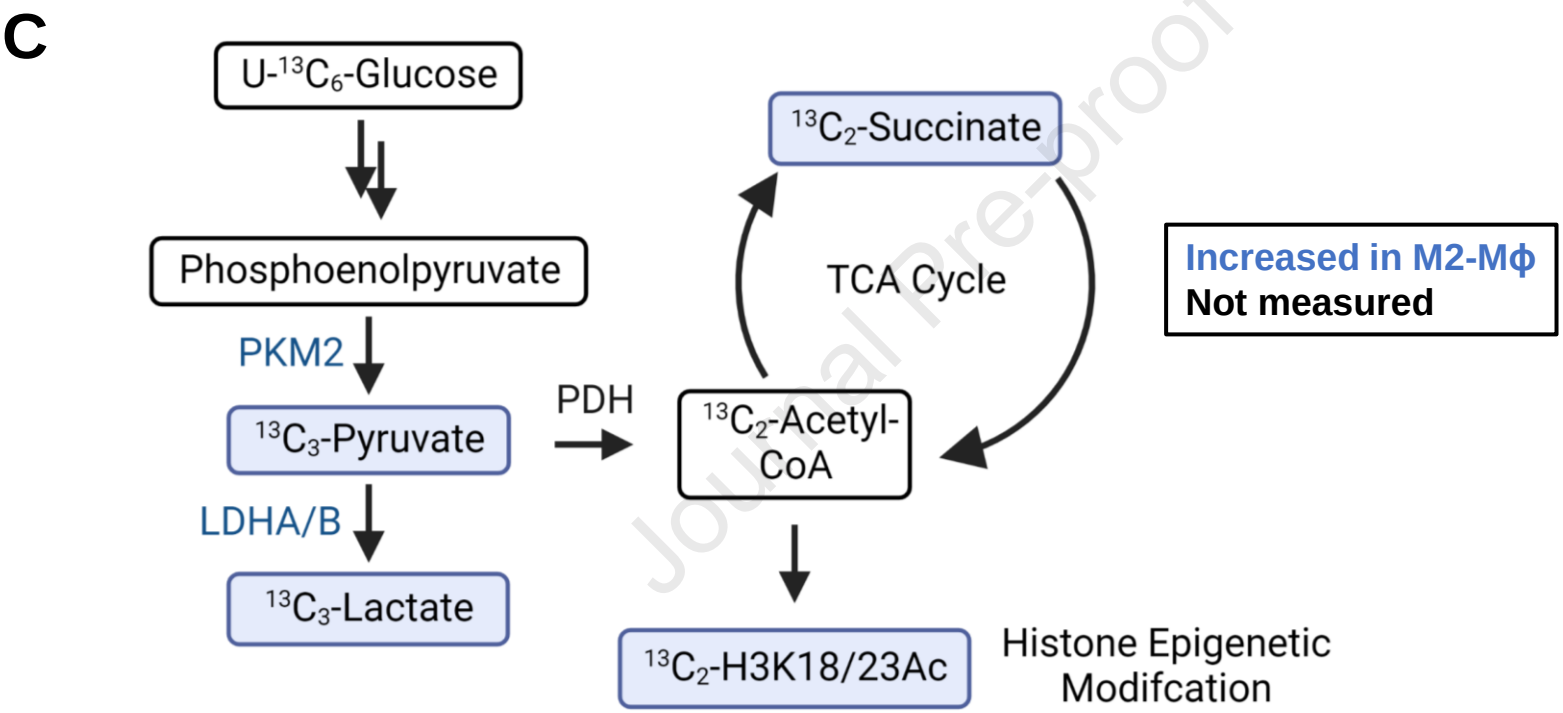

There is no conflict of interest.